



1 High-resolution spatial patterns and drivers of terrestrial 2 ecosystem carbon dioxide, methane, and nitrous oxide fluxes 3 in the tundra

4 Anna-Maria Virkkala^{1,2}, Pekka Niittynen³, Julia Kemppinen⁴, Maija E. Marushchak⁵, Carolina Voigt⁵,
5 Geert Hensgens⁶, Johanna Kerttula⁵, Konsta Happonen⁷, Vilna Tyystjärvi⁸, Christina Biasi⁵, Jenni
6 Hultman^{9,10}, Janne Rinne⁹, Miska Luoto²

7 ¹Woodwell Climate Research Center, Falmouth, 149 Woods Hole Road, MA, USA

8 ²University of Helsinki, Department of Geosciences and Geography, Gustaf Hällströmin katu 2,
9 00014 University of Helsinki, Finland

10 ³University of Jyväskylä, Department of Biological and Environmental Science, P.O. Box 35 FI-
11 40014, Jyväskylä, Finland

12 ⁴Geography Research Unit, University of Oulu, P.O. Box 8000 FI-90014, Oulu, Finland

13 ⁵University of Eastern Finland, Department of Environmental and Biological Sciences, P.O. Box 1627
14 FI- 70211, Kuopio, Finland

15 ⁶Vrije Universiteit Amsterdam, Department of Earth and Climate, De Boelelaan 1085, 1081 HV,
16 Amsterdam, the Netherlands

17 ⁷Youth Research Society, Kumpulantie 3 A, 00520 Helsinki, Finland

18 ⁸Finnish Meteorological Institute, Climate System Research Unit, Erik Palménin aukio 1, FI-00560
19 Helsinki, Finland

20 ⁹Natural Resources Institute Finland, Latokartanonkaari 9, 00790 Helsinki, Finland

21 ¹⁰University of Helsinki, Department of Microbiology, Viikinkaari 9, 00014 University of Helsinki,
22 Finland

23 *Correspondence to:* Anna-Maria Virkkala, avirkkala@woodwellclimate.org

24 **Abstract.** Arctic terrestrial greenhouse gas (GHG) fluxes of carbon dioxide (CO₂), methane (CH₄) and nitrous
25 oxide (N₂O) play an important role in the global GHG budget. However, these GHG fluxes are rarely studied
26 simultaneously, and our understanding of the conditions controlling them across spatial gradients is limited.
27 Here, we explore the magnitudes and drivers of GHG fluxes across fine-scale terrestrial gradients during the
28 peak growing season (July) in sub-Arctic Finland. We measured chamber-derived GHG fluxes and soil
29 temperature, soil moisture, soil organic carbon and nitrogen stocks, soil pH, soil carbon-to-nitrogen (C/N) ratio,
30 soil dissolved organic carbon content, vascular plant biomass, and vegetation type from 101 plots scattered
31 across a heterogeneous tundra landscape (5 km²). We used these field data together with high-resolution remote
32 sensing data to develop machine learning models to predict (i.e., upscale) daytime GHG fluxes across the
33 landscape at 2-m resolution. Our results show that this region was on average a daytime net GHG sink during
34 the growing season. Although our results suggest that this sink was driven by CO₂ uptake, it also revealed small
35 but widespread CH₄ uptake in upland vegetation types, shifting this region to an average net CH₄ sink at the
36 landscape scale during growing season, despite the presence of high-emitting wetlands. Average N₂O fluxes
37 were negligible. CO₂ fluxes were controlled primarily by annual average soil temperature and biomass (both
38 increase net sink) and vegetation type, CH₄ fluxes by soil moisture (increases net emissions) and vegetation
39 type, and N₂O fluxes by soil C/N (lower C/N increases net source). These results demonstrate the potential of
40 high spatial resolution modelling of GHG fluxes in the Arctic. They also reveal the dominant role of CO₂ fluxes
41 across the tundra landscape but suggest that CH₄ uptake might play a significant role in the regional GHG
42 budget.



43 **1 Introduction**

44 Over the past millennia, Arctic soils in the treeless tundra biome have played an important role in the global
45 climate system by accumulating large amounts of carbon (C) and nitrogen (N), thus cooling the climate
46 (Hugelius et al., 2014, 2020; Strauss et al., 2017). However, the ongoing climate warming is changing the C and
47 N cycles, leading to potentially increased net greenhouse gas (GHG) emissions from Arctic ecosystems to the
48 atmosphere (Belshe et al., 2013; McGuire et al., 2012; Masyagina and Menyailo, 2020). Yet, even the current
49 GHG balance of Arctic ecosystems is insufficiently understood due to severe gaps in flux measurement
50 networks and poorly performing coarse-resolution models (Virkkala et al., 2021; Treat et al., 2018c). Thus, the
51 contribution of Arctic regions to the global climate feedback remains uncertain.

52 One of the main uncertainties in understanding the Arctic GHG balance is related to the inadequately quantified
53 magnitudes of all three main GHG fluxes - carbon dioxide (CO₂), methane (CH₄) and nitrous oxide (N₂O) -
54 which show pronounced spatial variability across the diverse terrestrial environmental gradients in tundra
55 (Virkkala et al., 2018; Pallandt et al., 2021; Voigt et al., 2020). In most tundra ecosystems, CO₂ fluxes are the
56 largest flux driving the GHG balance due to the strong growing season photosynthetic activity and relatively
57 high non-growing season respiratory CO₂ losses (Natali et al., 2019; Euskirchen et al., 2012; Heiskanen et al.,
58 2021). However, growing evidence points to the importance of CH₄ and N₂O fluxes, which are more potent
59 GHGs than CO₂ (Voigt et al., 2017b). These two trace gases can have considerable variation between sink and
60 source activity in the tundra, and they have different spatiotemporal dynamics with each other and compared to
61 CO₂ fluxes (Emmerton et al., 2014; Bruhwiler et al., 2021). However, only a few studies have simultaneously
62 considered the contributions of all three main GHG fluxes to the tundra GHG balance (Voigt et al., 2017b;
63 Kelsey et al., 2016; Brummell et al., 2012; Wagner et al., 2019).

64 The largest fine-scale differences in Arctic GHG fluxes occur in ecosystems with spatially varying soil moisture
65 conditions (McGuire et al., 2012). Broadly speaking, the Arctic can be divided into wetlands and drier uplands
66 (i.e., shrublands, grasslands, and barren lands; see e.g. (Treat et al., 2018a; Virkkala et al., 2021). Wetlands
67 cover between 5 and 25 % of the Arctic (Olefeldt et al., 2021; Kåresdotter et al., 2021; Raynolds et al., 2019).
68 They are hotspots for soil C and N stocks and have the potential for high CH₄ emissions (Euskirchen et al.,
69 2014; Hugelius et al., 2020); therefore they have been intensively studied (Rinne et al., 2018; Peltola et al.,
70 2019; Turetsky et al., 2014). However, uplands cover the largest part of the Arctic (75 to 95 %) and can have
71 significant variability in environmental conditions and GHG fluxes. These uplands have been relatively well
72 studied for CO₂ fluxes (Williams et al., 2006; Cahoon et al., 2012a). Upland CH₄ and N₂O fluxes, on the other
73 hand, remain less well understood in terms of their magnitudes and drivers (Virkkala et al., 2018; Voigt et al.,
74 2020). There are still likely some GHG flux hotspots to be discovered and coldspots to be verified, particularly
75 in the upland tundra ecosystems.

76 The Arctic tundra is characterised by fine-scale environmental heterogeneity even within upland and wetland
77 tundra environments. Thus, local-scale study settings that cover the main spatial environmental gradients are
78 highly important (Treat et al., 2018c; Davidson et al., 2017). Such fine-scale variabilities are often measured
79 with chambers, but most chamber-based study designs are limited to relatively small environmental gradients
80 focusing on only a handful of different land cover types and environmental variables, leaving large gaps in our



81 understanding of GHG flux hotspots (Virkkala et al. 2018). In this study, using an extensive spatial study design
82 with chamber GHG flux measurements from 101 plots, we aim to understand the magnitudes and environmental
83 drivers of Arctic terrestrial CO₂, CH₄, and N₂O fluxes in a heterogeneous tundra landscape dominated by upland
84 heaths. By combining in-situ measurements and remote sensing data, we investigate the fine-scale (2 m) spatial
85 heterogeneity of GHG fluxes across the landscape, and estimate the contribution of the three gases to the total
86 landscape-scale GHG flux.

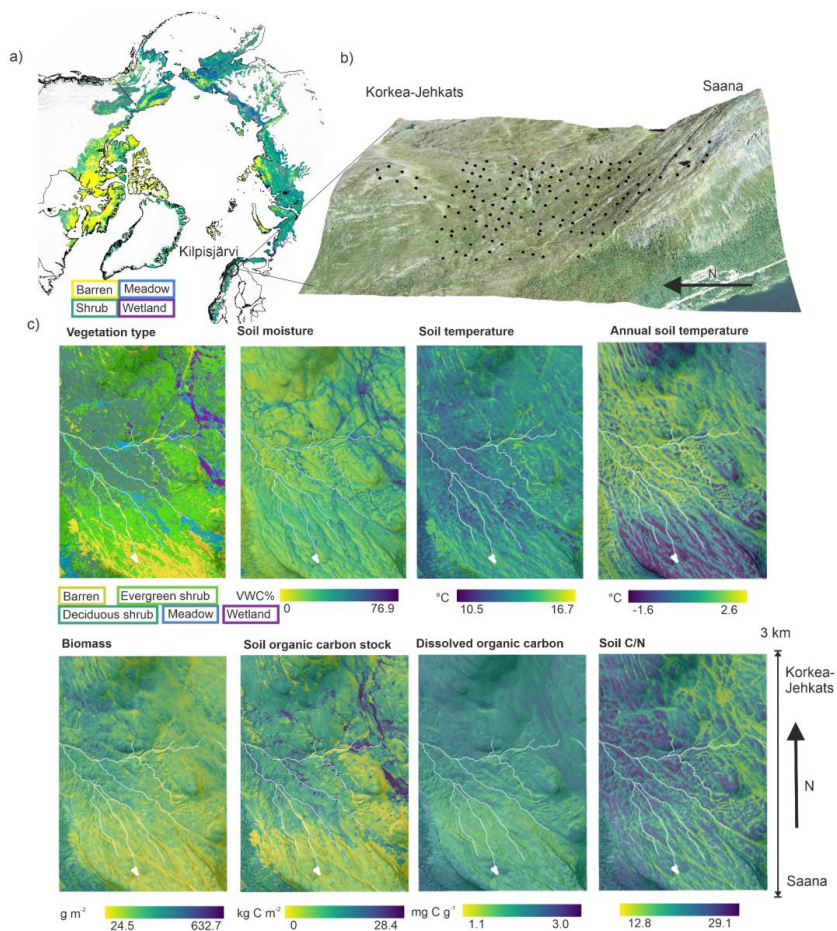
87

88 **2 Materials and Methods**

89 **2.1 Study area**

90 The field measurements were collected during 2016-2018 in a sub-Arctic tundra environment in Kilpisjärvi
91 (Gilbbesjávri in Northern Sámi language), northwestern Finland (69.06 N, 20.81 E). The study area is located on
92 an elevational gradient between two fells, Saana (Sána; 1029 m.a.s.l.) and Korkea-Jehkats (Jiehkkaš; 960 m.a.s.l.),
93 and the valley in between (~600 m.a.s.l.). The study area is above the mountain birch (*Betula pubescens* ssp.
94 *czerepanovii*) forest and is dominated by dwarf-shrub evergreen and deciduous heaths. Dominant vascular plant
95 species are, e.g., *Empetrum nigrum* ssp. *hermaphroditum*, *Betula nana*, *Vaccinium myrtillus*, *Vaccinium vitis-*
96 *idaea*, and *Phyllodoce caerulea*. Vegetation in the wetlands is dominated by species common to fen wetlands,
97 such as *Eriophorum* sp. or *Carex* sp. Mesic meadows are rich in forbs and grasses whereas barren heaths
98 accommodate mostly lichens (e.g. *Cladonia* spp.) and mat-forming cushion plants (e.g. *Diapensia lapponica*) with
99 scattered patches of *E. nigrum* and *B. nana*. Soils in the area are shallow (mean organic layer depth 6.6 cm, mean
100 mineral layer depth 13.0 cm), and permafrost is absent from soils but can be found in the bedrock above 800 m
101 a.s.l. (King and Seppälä, 1987). The environment is relatively undisturbed but experiences reindeer (*Rangifer*
102 *tarandus tarandus*) grazing. The mean annual temperature in Saana fell (1002 m.a.s.l.) is -3.1 °C and the annual
103 precipitation in Kilpisjärvi village ca. 5 km from the study site (480 m.a.s.l.) is 518 mm in 1991-2018 (Finnish
104 Meteorological Institute, 2019a, b).

105 Our study design covered an area of ca. 3 x 1.5 km and consisted of 101 GHG flux measurement plots and 50 to
106 5280 plots with other environmental data (Fig. 1). We selected the plots based on a combination of stratified
107 sampling and systematic grid approaches, and the plots contain a variety of environmental gradients and habitats
108 as well as the transition zones between them (Kempinen et al., 2021). We recorded the locations of the plots
109 using a hand-held Global Navigation Satellite System receiver with an accuracy of up to ≤6 cm under optimal
110 conditions (GeoExplorer GeoXH 6000 Series; Trimble Inc., Sunnyvale, CA, USA).



111
112 **Figure 1:** The distribution of the main vegetation types across the Arctic tundra (Dinerstein et al., 2017; Agency,
113 2017) and the location of our study area (a), the distribution of plots (b) and environmental conditions derived
114 from statistical upscaling of in-situ measurements (see Sect. 2.4.2 Machine learning models) across the study area
115 (c). Soil moisture and temperature represent mean daytime (8 am to 8 pm) conditions from the 1st of July to the
116 2nd of August and annual soil temperature is an average within the entire year (July 2017-June 2018). Other
117 conditions represent growing season conditions and are considered static in this study. The aerial image is
118 produced by the National Land Survey of Finland (accessed in 2016).

119 2.2 Data

120 We measured GHG fluxes from 101 plots during the peak growing season (from now on, growing season).
121 Environmental conditions explaining these GHG fluxes were measured from 73-100 % of these plots; missing
122 data were filled using the environmental predictions (see Sect. 2.4.2 Machine learning models, Table S1). We
123 used additional in-situ environmental data to upscale and visualize environmental conditions across the entire



124 landscape (see Sect. 2.4.2 Machine learning models and Fig. 2): continuous soil moisture loggers (50 plots),
125 continuous soil temperature loggers (250), soil samples for carbon and nitrogen stock and C/N estimation (168),
126 and vegetation classification data (5280). The full set of variables at a plot consisted of the plot for GHG flux
127 measurements, and of a nearby complementing plot (max. 2 m distance) where we monitored soil moisture and
128 temperature continuously and did a vegetation classification. The additional plot was separated from the GHG
129 plot to avoid disturbance of the continuous recordings. The additional plot was carefully situated to similar
130 vegetation and microtopographic conditions as the GHG plot. Soil samples were collected as close as possible to
131 the GHG plot.

132 2.2.1 Chamber measurements

133 We measured GHG exchange using a static, non-steady state non-flow-through system (Livingston and
134 Hutchinson, 1995) composed of an acrylic chamber (20 cm diameter, 25 cm height). The chamber was placed
135 on top of a collar and ventilated before each measurement. Prior to the measurements, we installed steel collars,
136 which were 21 cm in diameter and 6-7 cm in height. Each collar was visited once during the growing-season ,
137 and measurements were conducted between 10 am and 5 pm. Although we did not have any temporal replicates,
138 the spatial variation in our plots covered most of the temperature variation during the growing season. For more
139 details, see Sect. S1.

140 For CO₂ flux measurements, transparent and opaque chamber measurements were conducted during 1st of July
141 and 27th of July, 2018. The chamber included a small fan, a carbon dioxide probe GMP343 and an air humidity
142 and temperature probe HMP75 (Vaisala, Finland). In the chamber, CO₂ concentration, air temperature and
143 relative air humidity were recorded at 5-s intervals for 90 s. Photosynthetically active radiation was logged
144 manually outside the chamber at 10-s intervals during the same period using a MQ-200 quantum sensor with a
145 hand-held meter (Apogee Instruments, Inc, USA). MQ-200 measures photosynthetic photon flux density
146 (PPFD) at a spectral range from 410 to 655 nm in $\mu\text{mol m}^{-2} \text{s}^{-1}$. For more details of the equipment, see
147 Happonen et al. (2022).

148 We progressively decreased the light intensity of net ecosystem exchange (NEE) measurements from ambient
149 conditions to ca. 80%, 50% and 30% PPFD by shading the chamber with layers of white mosquito net (replicate
150 measurements per collar = 5 - 9). Ecosystem respiration (ER) was measured in dark conditions (0 PPFD), which
151 were obtained by covering the chamber with a space blanket (replicates = 2 - 3). Before flux calculations, we
152 discarded the first 0 - 5 s as well as the last 5 s of the measurements to remove potentially disturbed
153 observations. Fluxes were calculated from the concentration change within the chamber headspace over time
154 using linear regression (for performance statistics see Sect. S2).

155 We standardized NEE, GPP, and ER measurements conducted at different light and temperature conditions to
156 allow across-plot comparison of the fluxes. We fitted light-response curves using a non-linear hierarchical
157 bayesian model with the plot as a random effect (Sect. S5). We used the Michaelis-Menten equation to model
158 instantaneous NEE as a function of plot-specific ER, maximum photosynthetic rate (GPP_{max}) and the half-
159 saturation constant (K) using the same formula as in (Williams et al., 2006; Cahoon et al., 2012b). ER also had
160 an exponential air temperature (T) response (for more details, see (Happonen et al., 2022). We used this model



161 to predict NEE at dark (0 PPFD, i.e. ER) and average light (600 PPFD) conditions, and an air temperature of
162 20°C at each plot. 20°C was chosen as it represents a typical air temperature inside the chamber during flux
163 measurements, and 600 PPFD because it is widely used in tundra literature (Dagg and Lafleur, 2011; Shaver et
164 al., 2007). We then subtracted ER from the NEE normalized to average light conditions to arrive at an estimate
165 of normalized gross primary productivity (GPP). Negative values in NEE indicate a net sink of CO₂ from the
166 atmosphere to the ecosystems. GPP and ER are given as positive values.

167 We measured CH₄ and N₂O fluxes with an opaque chamber (0 PPFD). Measurements were conducted during
168 the 2nd of July and 2nd of August, 2018. Five gas samples were taken within a 50-min enclosure time and
169 transferred into 12-mL vials (Labco Exetainer, Labco Ltd.). The vials were pre-evacuated in the laboratory and
170 filled with 25 mL of the sample in the field. Gas samples were analyzed at the University of Eastern Finland
171 with a gas chromatograph (Agilent 7890B; Agilent Technologies, Santa Clara, CA, USA), equipped with an
172 autosampler (Gilson Inc., Middleton, WI, USA), with thermal conductivity detector (TCD) for CO₂, flame
173 ionization detector (FID) for CH₄ and an electron capture detector (ECD) for N₂O. We calculated gas
174 concentrations from GC peak areas relative to peak areas derived by analyzing gas standards (CO₂: 7
175 concentration levels ranging from 0-10000 ppm; CH₄: 7 concentration levels ranging from 0-100 ppm; N₂O: 5
176 concentration levels ranging from 0-5000 ppb). Fluxes were calculated from the concentration change within the
177 chamber headspace over time using linear regression. Quality control was based on visual inspection and
178 RMSE. We also verified that the RMSE was less than 3 * standard deviation of gas standards in a similar
179 concentration range. Negative values in these fluxes represent net CH₄ and N₂O sinks from the atmosphere to
180 the ecosystems.

181 2.2.2 Soil temperature and moisture data

182 Soil moisture and soil temperature were measured simultaneously during the flux measurements. We measured
183 soil moisture with a time-domain reflectometry sensor (FieldScout TDR 300; Spectrum Technologies Inc.,
184 Plainfield, IL, USA; 0 to 7.5 cm depth). Soil temperature measurements conducted at the same time as CO₂ flux
185 measurements were taken with a thermometer (TD 11 thermometer; VWR International bvba; Leuven,
186 Germany; 6.0 to 7.5 cm depth). Soil temperature measurements (TM-80N measure and ATT-50 sensor)
187 conducted at the same time as CH₄ and N₂O flux measurements were taken with a thermometer in the uppermost
188 10 cm. We refer to these variables as soil moisture and soil temperature throughout the text.

189 Temperature loggers (Thermochron iButton DS1921G and DS1922L, San Jose, CA, USA and TMS-4; TOMST
190 s.r.o., Prague, Czech Republic) monitored temperatures at 7.5 cm and 6.5 cm (iButton and TMS-4, respectively)
191 belowground at 0.25–4 h intervals (Sect. S3). We calculated a variable describing soil temperature conditions
192 during the previous 12 months by averaging the iButton measurements from the study design (n=138) from July,
193 2017 to June 2018. We refer to this variable as annual soil temperature. In addition to temperature, the TMS-4
194 loggers also monitored soil moisture (raw time-domain transmission data between 1 and 4095) to a depth of c.
195 14 cm (Wild et al., 2019). The raw time-domain transmission data was transformed into volumetric water
196 content (VWC%) (Tyystjärvi et al., 2022).



197 These continuous soil moisture and temperature data were used to upscale soil microclimatic conditions at 2-
198 hour timesteps during daytime (8 am to 8 pm) and from the 1st of July to the 2nd of August (see section Models
199 used to predict environmental conditions). This period was chosen because the GHG fluxes were measured
200 during this period and we did not want to extrapolate outside our main measurement campaign. Moreover, this
201 period represents the peak growing season of this region.

202 2.2.3 Vegetation data

203 We took images from CH₄ and N₂O collars on the measurement day and used them to classify the dominant
204 vegetation to five distinct classes, following the Circumpolar Arctic Vegetation Map physiognomic
205 classification system (Walker et al. 2005) with minor modifications (Fig. 1). We used the following classes:
206 barren (< 10 % vegetation cover), meadow (graminoids and forbs), evergreen shrub, deciduous shrub, and
207 wetlands. We also utilized a larger dataset of 5820 vegetation descriptions from the study design to create the
208 vegetation type map.

209 We collected biomass samples from above-ground vascular plants using the clip-harvest method during late
210 peak season, between 17th of July and 10th of August. Samples were collected within the chamber collars, and
211 were oven-dried at 70°C for 48 h and weighed after drying. We refer to this variable as biomass (g dry-weight
212 m⁻²).

213 2.2.4 Soil sampling and analyses

214 We measured the thickness of the organic and mineral soil layers using a metal probe reaching up to 80 cm
215 depth. We collected soil samples (ca. 1 dl) from the organic and mineral layers using metal soil core cylinders (4
216 - 6 cm Ø, 5 - 7 cm height) during August in 2016-2018. The organic samples were collected from the top soil,
217 and mineral samples directly below the organic layer which was on average 6.6 cm deep. Large roots were
218 excluded from the samples. The soil samples were freeze-dried and analysed in the Laboratory of Geosciences
219 and Geography and Laboratory of Forest Sciences (University of Helsinki). Bulk density (kg m⁻³) was estimated
220 by dividing the dry weight by the sample volume. Soil organic layer pH was analyzed following ISO standard
221 10390. Total carbon and nitrogen content (C%, N%) analyses were done using Vario Elementar Micro cube and
222 Vario Elementar Max -analyzer (Elementar Analysensysteme GmbH, Germany). Prior to CN% analysis,
223 mineral samples were sieved through a 2 mm plastic sieve. Organic samples were homogenized by hammering
224 the material into smaller pieces.

225 Soils in this landscape are acidic and likely have a minimal amount of carbonates; consequently, we assumed
226 C% to equal organic C%. Soil organic carbon and nitrogen stocks were calculated for the entire soil horizon up
227 to 80 cm (in 95 % of plots soil depth was less than that). Some plots lacked CN% data (30 % of the plots), and
228 therefore, we used soil organic matter content estimated with the loss-on-ignition method according to SFS 3008
229 (1990). We utilized a similar stock calculation framework using the bulk density, layer depth, and C% and N%
230 data as in Kemppinen et al. (2021) except we used average bulk density and mineral C% estimates in each
231 vegetation type in case that information was missing in stock calculation.



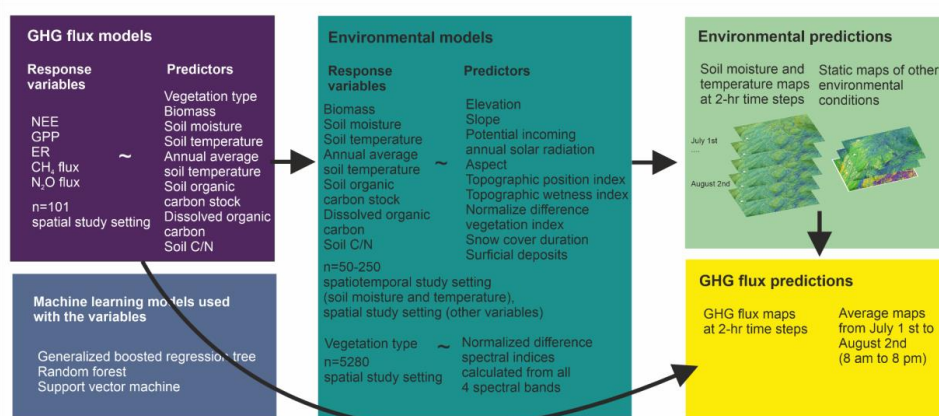
232 Soil samples for dissolved organic carbon concentration analyses in dry soil were collected between the 5th and
 233 14th of July 2018. After the collection, samples were stored at 4 °C and then dried at 60 °C for at least 5 days.
 234 Extraction of dissolved organic carbon was done using pure water extractions with 0.5 to 3 grams of dried soil
 235 added to 40 ml of water following the WEOC protocol from (Hensgens et al., 2021). Extracts were immediately
 236 filtered (0.7µm) using glass fibre filters, diluted, acidified to remove inorganic carbon, and measured on a
 237 Shimadzu TOC V-CPN analyzer set on the Nonpurgeable Organic Carbon mode. We refer to this variable as
 238 dissolved organic carbon.

239 2.2.5 Remotely sensed data

240 Remotely sensed optical and light detection and ranging-based (LiDAR) data describing topographic,
 241 vegetation, snow, and surficial deposit conditions was used for upscaling the in-situ measured environmental
 242 variables (Fig. 2, Sect. S4 and Fig. S1).

243 2.3 Statistical analyses

244 We investigated the dependencies of GPP, ER, NEE, CH₄ flux, and N₂O flux on environmental variables using
 245 statistical analyses which included analysis of variance (ANOVA), and machine learning modeling and
 246 prediction. We developed machine learning models, in which we 1) upscaled environmental data (annual soil
 247 temperature, soil temperature, soil moisture, soil C/N, soil organic carbon stock, dissolved organic carbon,
 248 biomass) using remotely sensed variables as predictors; 2) modeled GHG fluxes using the environmental data as
 249 predictors, and 3) upscaled GHG fluxes using the upscaled environmental data maps at a 2-meter spatial
 250 resolution across the landscape (Fig. 2). This two-step upscaling approach enabled us to focus on the
 251 relationships between GHG fluxes with their physical and ecological, in-situ measured environmental controls
 252 instead of the remotely sensed data that are proxies by nature. We ran all analysis in the R statistical
 253 programming environment (R Core Team 2020; version 4.0.3).
 254



255



256 **Figure 2:** The upscaling framework used in this study. We first linked GHG fluxes to the in-situ environmental
257 drivers using machine learning models. Then we trained three machine learning models to upscale environmental
258 conditions across the landscape using remote sensing data. Then we used the GHG flux models and environmental
259 predictions to upscale GHG fluxes across the landscape throughout the entire growing season.

260 2.3.1 Analysis of variance (ANOVA)

261 We used one-way ANOVAs to test for vegetation type differences in environmental conditions, GHG fluxes,
262 and tested significance using multiple comparisons with a Tukey's honest significant difference test ($p < 0.05$).
263 CH₄ flux, soil moisture, soil organic carbon and nitrogen stock, and biomass were not normally distributed, thus
264 we used Kruskal-Wallis test instead of ANOVA at first.

265 2.3.2 Machine learning models

266 We modeled our response variables using three machine-learning methods (generalized boosted regression
267 models, GBM; random forest, RF, and support vector machine regression, SVM), all of which have been widely
268 used in flux upscaling studies (see e.g. Natali et al., 2019; Peltola et al., 2019; Tramontana et al., 2016). Based
269 on these models, we visualized the partial dependence plots characterizing the relationships between the
270 response and predictor variables while accounting for the average effect of the other predictors in the model
271 using the pdp package (Greenwell, 2017). Further, we calculated variable importance using the vip package
272 (Greenwell et al., 2020). Variable importance scores were estimated by randomly permuting the values of the
273 predictor in the training data and exploring how this influenced model performance based on the adjusted R²
274 values, with the idea that random permutation would decrease model performance (Breiman, 2001). For more
275 details, see Sect. S5.

276 We used ten topography, snow, vegetation, and surficial deposits variables to construct landscape-wide
277 predictors matching the in-situ environmental conditions that we used to model the GHG flux values. These
278 variables were the following: elevation, topographic wetness index, topographic position index at 5 and 30 m
279 radii, aspect, slope, potential incoming solar radiation, normalized difference vegetation index, snow cover
280 duration, and surface deposits. Soil organic carbon stocks, dissolved organic carbon, soil C/N, biomass, and
281 annual soil temperature models were calibrated only once and a single prediction was made to the landscape.
282 Soil temperatures and moisture vary throughout the growing season, thus, we calibrated each model at each time
283 step and created 231 predictions over the study period (every 2 hours between 8 am and 8 pm from July 1st until
284 August 2nd). For each variable, an ensemble prediction was produced by calculating a median prediction over
285 the three predictions from the different modeling methods. Soil organic carbon stock was log+1 and biomass
286 were log-transformed prior to tuning the models, and after making the predictions, values were transformed
287 back to the original scale.

288 We examined the relationship between the five primary response variables (GPP, ER, NEE, CH₄ flux, N₂O flux)
289 and environmental predictors that describe (i) soil resources and conditions (soil moisture, soil C/N, soil pH)
290 which are relevant to, for example, the growth of organisms (Nobrega and Grogan, 2008; Happonen et al.,
291 2022); (ii) soil C and N stocks and dissolved organic carbon which are one of the main sources for the GHG



292 emissions (Bradley-Cook and Virginia, 2018); (iii) soil temperatures which regulate enzymatic processes (St
293 Pierre et al., 2019; Mauritz et al., 2017); and (iv) biomass and vegetation type which describe resource-use
294 strategies, carbon inputs to soils and plant photosynthetic capacity, and integrate multiple environmental
295 properties into one variable (Magnani et al., 2022). We excluded soil pH and soil nitrogen stock from modeling
296 analyses due to high correlations (Pearsons's $r > 0.7$) with soil moisture and soil organic carbon stock,
297 respectively. We did not use air temperature as a predictor as we already controlled for it in CO₂ fluxes in the
298 light-response model, and we assumed that soil microbes regulating CH₄ and N₂O cycling are most importantly
299 driven by soil temperatures (Kuhn et al., 2021). The final predictors for our models were soil moisture, soil
300 temperature, annual soil temperature, soil organic carbon stock, dissolved organic carbon, soil C/N, biomass,
301 and vegetation type. After exploring the distribution of residuals of the preliminary GHG flux models, we
302 transformed CH₄ fluxes with cube-root transformation, and soil moisture with log transformation prior to tuning
303 the CH₄ flux model; in other models transformations were not necessary. The machine learning parameters
304 tuned for each model can be found from Sect. S5.

305 We used the machine learning models to predict GHG fluxes across the landscape for each 2-hour time step
306 from July 1st until August 2nd. Similar to the environmental predictions, an ensemble prediction was produced
307 by calculating a median prediction over the three predictions from the different modeling methods. As our focus
308 was on understanding the spatial patterns in the mean growing season fluxes, we averaged GHG flux predictions
309 over the study period. However, a visualization of the predicted mean daily patterns in soil moisture and
310 temperatures, and the consequent GHG fluxes is provided in the supplementary material (Fig. S2).

311 To compare the magnitude of all three important GHGs, namely CO₂, CH₄, and N₂O, we calculated the radiative
312 forcing strength of the three GHGs over a 100-year period from our measurements and ensemble predictions.
313 We used the Global Warming Potential (GWP; 27 for CH₄ and 273 for N₂O (IPCC 2021)) and sustained GWP
314 (45 for CH₄ and 270 for N₂O (Neubauer 2015), which are, to our knowledge, the best and most widely used
315 approaches that exist to compare flux magnitudes. We acknowledge that these approaches are designed to
316 quantify an effect of a change in emission to the radiative forcing, and are thus not fully suitable to be used to
317 quantify the climatic effect of natural continuous fluxes in our study (Mathijssen et al., 2022; Frolking et al.,
318 2006).

319

320 For all of our models, we used a leave-one-plot-out cross validation scheme in which each plot was iteratively
321 left out from the data set, and the remaining data were used to predict fluxes for the excluded plot to assess the
322 predictive performance of the models (Bodesheim et al., 2018). Estimates of bias were calculated as an average
323 of the absolute error (MAE) between prediction and actual observation. Coefficient of determination (R^2) was
324 used to determine the strength of the linear relationship between the observed and predicted fluxes.

325 The root mean squared error (RMSE) was used to estimate the model error. Uncertainty in GHG flux
326 predictions was derived by bootstrapping (fractional resampling with replacement based on vegetation type
327 classes). We subset the model training data into 30 different data sets, all of which had the same number of
328 observations as the original data itself. These 30 data sets were then used to produce 30 individual predictions
329 for a subset of the times with all three machine learning models and their ensemble for each response variable
330 (Sect. S5). The uncertainty estimates represent how different distributions of the input data as well as model
331 parameters influence the upscaled flux maps.



332

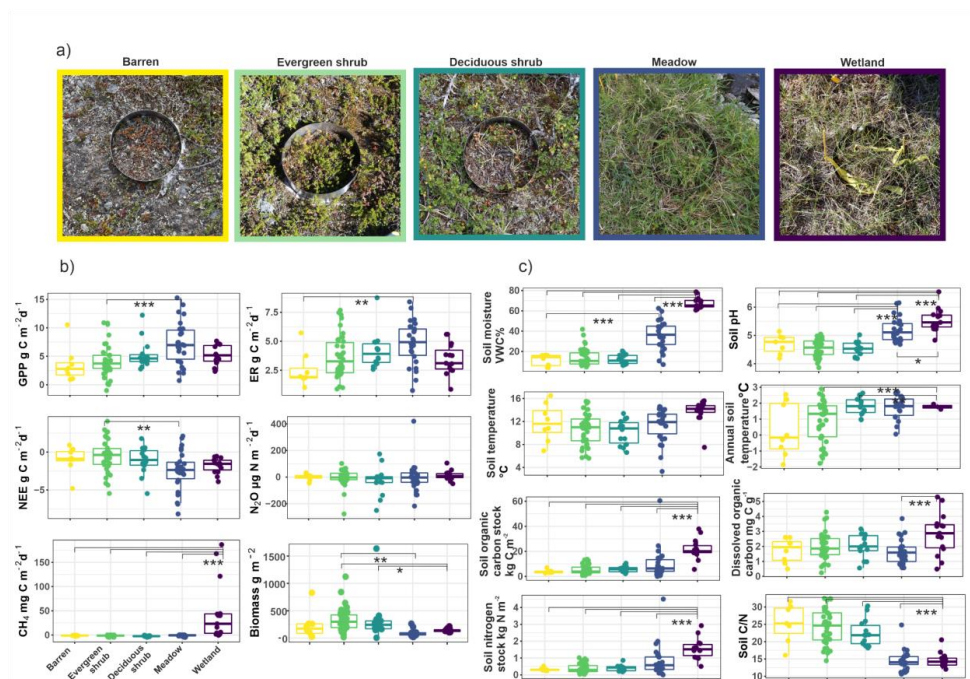
333 3 Results

334 3.1 Environmental conditions and GHG fluxes across vegetation types

335 We observed large variability in GHG fluxes and environmental conditions within and across vegetation types
336 (Fig. 3, Table S2). The variability in the different vegetation types differed depending on the flux and
337 environmental variable considered (e.g., meadow class had large variability in GPP and evergreen shrub class in
338 soil C/N). Frequently, wetlands differed clearly from the other vegetation types. While wetlands had high CH₄
339 emissions, all the other vegetation types with significantly lower soil moisture showed CH₄ uptake. Meadows
340 were a significantly larger net CO₂ sink than evergreen shrub sites, while other vegetation types had
341 intermediate NEE values. The N₂O fluxes were low from all vegetation types, and varied between small sinks
342 and small sources.

343

344



345

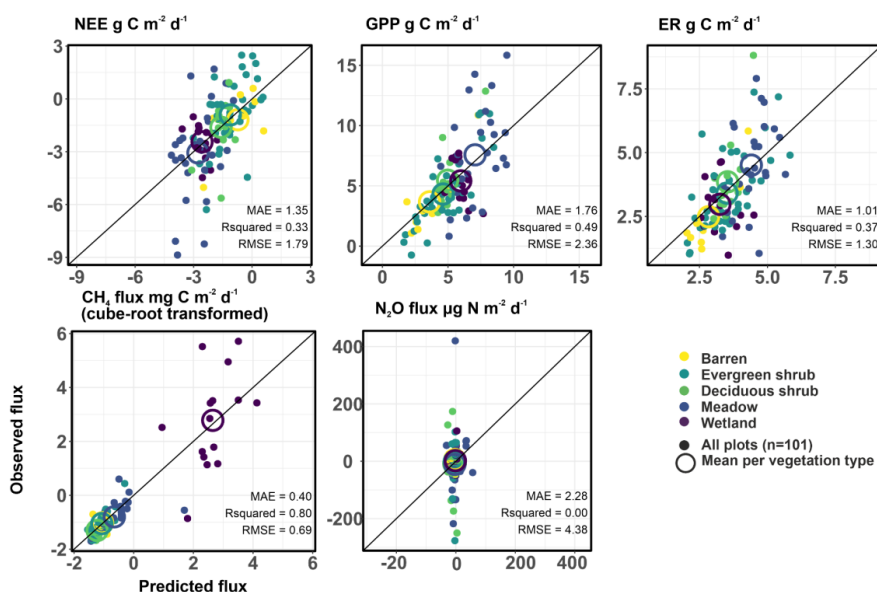
346 **Figure 3:** The vegetation types considered in this study (a), the distribution of GHG fluxes and biomass (b), and
347 environmental conditions (c) across the vegetation types. Lines represent Tukey's test results (* = $p \leq 0.05$, ** =
348 $p \leq 0.01$, *** = $p \leq 0.001$). The box corresponds to the 25th and 75th percentiles, and the line within the box
349 represents the median. The lines denote the 1.5 IQR of the lower and higher quartile, where IQR is the inter-
350 quartile range, or distance between the first and third quartiles.

351



352 3.2 The performance of environmental and greenhouse gas flux models

353 The predictive performance of the ensemble environmental variable models was rather high but varied
354 depending on the variable (R^2 : 0.43-0.71 except for soil temperature and soil dissolved organic carbon <0.26;
355 Fig. S3). The predictive performance of the GHG models was for most variables lower (R^2 : 0.00-0.80), with
356 N_2O flux models being close to random and CH_4 models performing the best (Fig. 4). The scatterplots of
357 observed and predicted GHG fluxes suggest that the highest flux estimates are often predicted most poorly, but
358 the mean fluxes in each vegetation type were predicted accurately.
359



360
361

362 **Figure 4:** The correlation between observed and predicted values based on the ensemble model predictions (i.e.
363 median of the three machine learning model outputs). Model predictive performance is described with mean
364 absolute error (MAE), R^2 (Rsquared), and RMSE (root mean square error).

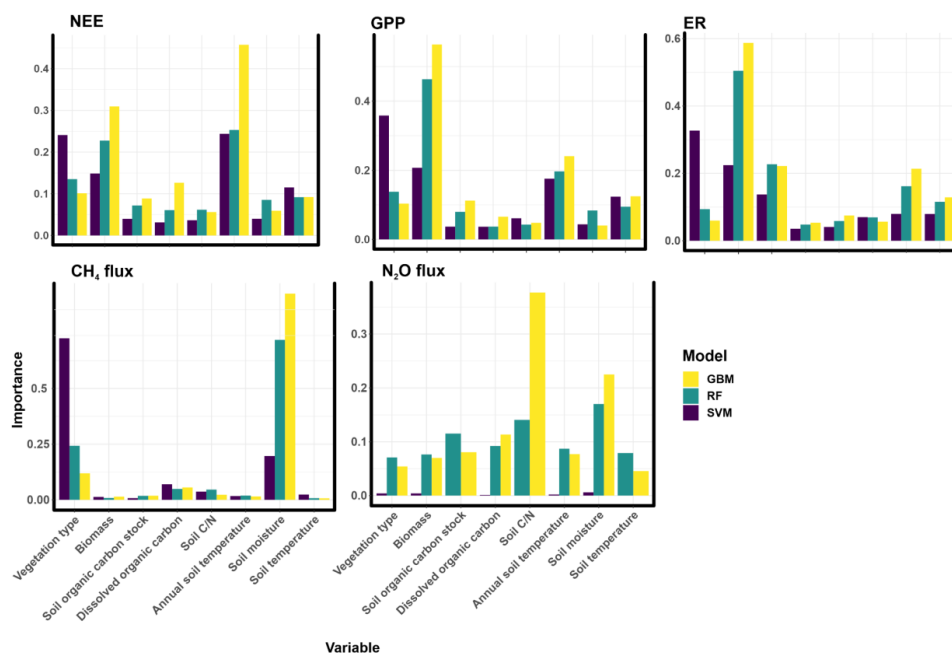
365 3.3 Drivers of greenhouse gas fluxes

366 The most important controlling variables and the response shapes differed depending on the GHG flux (Fig. 5,
367 Fig. 6 and Fig. S4), and sometimes also depending on the machine learning model type applied. CO_2 fluxes
368 were driven by annual average soil temperature, biomass, and vegetation type. In addition, soil organic carbon
369 stocks were an important predictor for ER. Soil moisture and vegetation type were the most important predictors
370 for CH_4 fluxes, and soil C/N and soil moisture for N_2O fluxes. In general, warmer and wetter conditions
371 increased net emissions of CH_4 and N_2O and net sink of CO_2 . Some fluxes were further positively correlated
372 with soil organic carbon stocks (ER, CH_4 flux) and negatively with soil C/N (GPP, ER, N_2O).

373

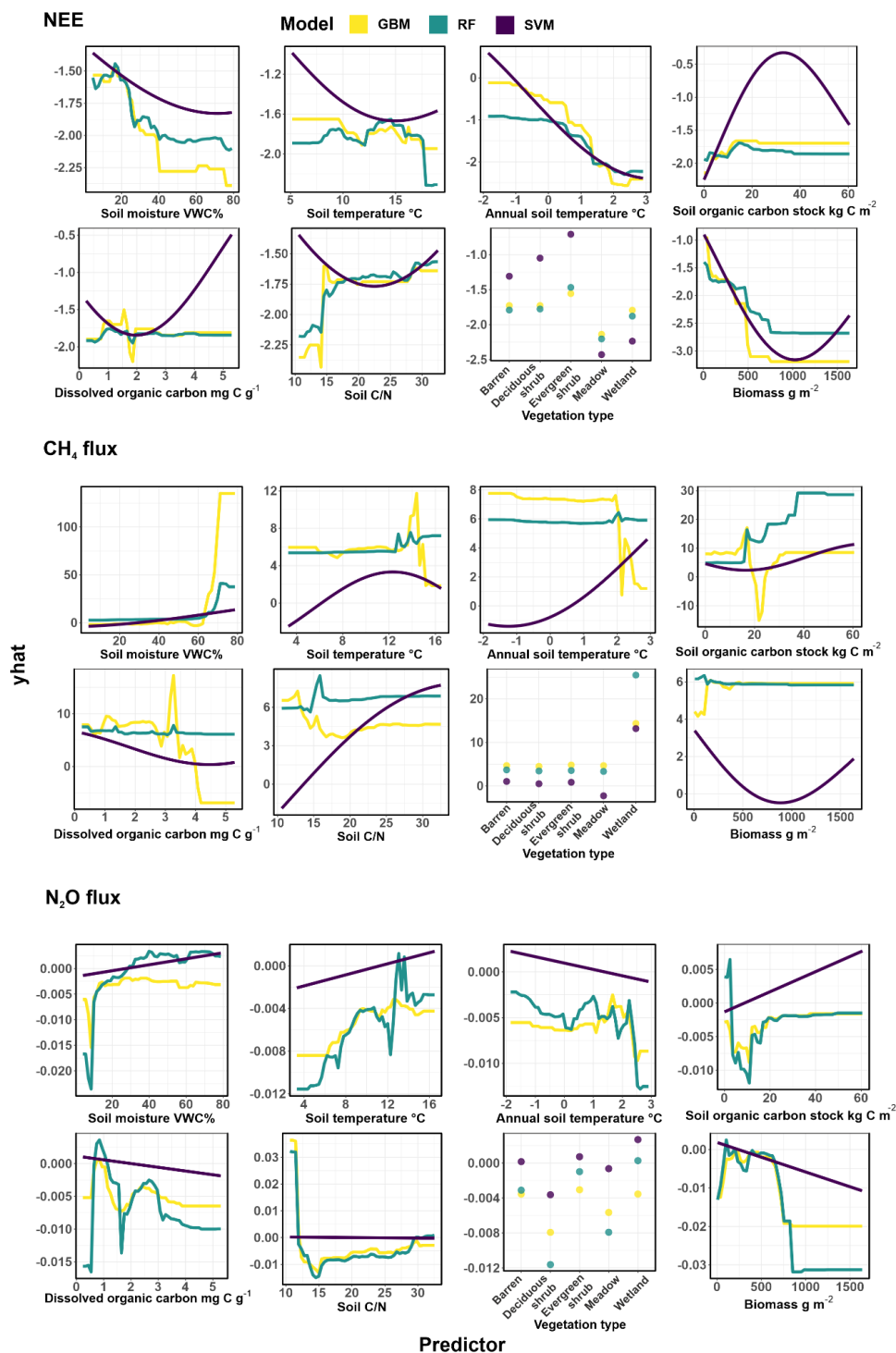


374
375



376
377
378
379

Figure 5: The variable importance of the environmental variables used to predict GHG fluxes. The models were generalized boosted regression models (GBM), random forest (RF), and support vector machine regression (SVM).

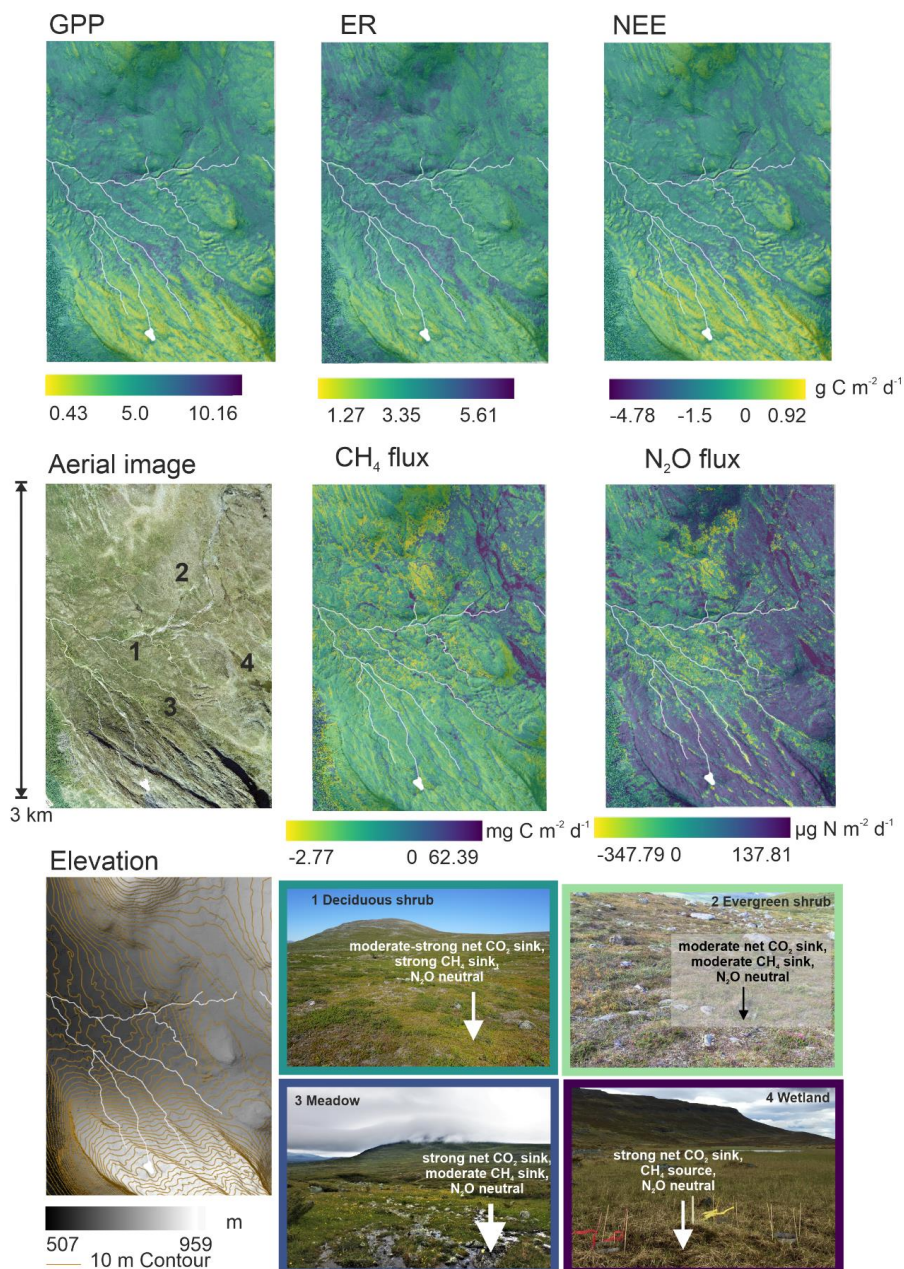




381 **Figure 6:** Partial dependence plots showing the relationships between GHG fluxes and environmental
382 conditions across the three models (generalized boosted regression models, GBM; random forest, RF; and
383 support vector machine regression, SVM). The y-axis of the plot (\hat{y}) represents the marginal effect of the
384 predictor on the response and should not be directly compared with observed or predicted values, rather the
385 shape and direction of the response instead. Partial dependence plots for GPP and ER are found in Fig. S4.

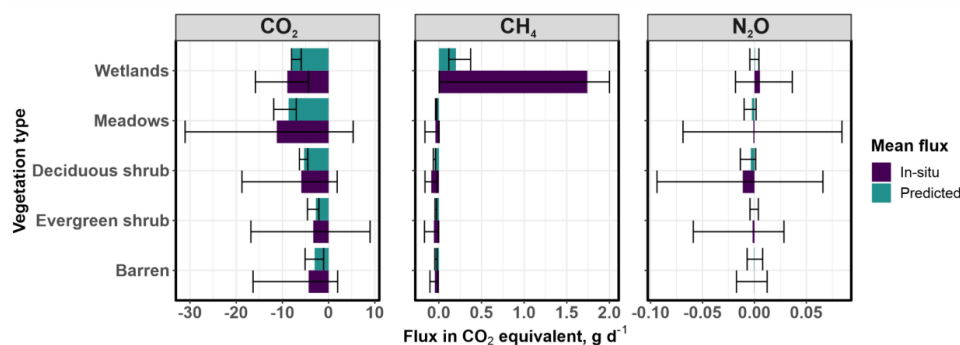
386 **3.4 Spatial patterns and contributions in greenhouse gas flux predictions**

387 The model predictions show large spatial variability in GHG fluxes across the landscape (Fig. 7, Fig. S5). Net
388 CO₂ uptake as well as GPP and ER were highest in the warm and productive meadow locations of the valley
389 whereas CH₄ and N₂O fluxes were highest in the eastern parts of the landscape that is dominated by wetlands.
390 The prediction suggests small but widespread net CH₄ uptake across the entire upland region. CO₂ was the most
391 important flux contributing to the net GHG sink (Fig. 8). Mean fluxes calculated based on the upscaled flux
392 maps differ from the in-situ based ones, particularly for wetland CH₄ emissions (Fig. 8, Fig. S6).





394 **Figure 7:** Ensemble predictions of growing season GHG fluxes, averaged over the 1st of July to the 2nd of
395 August (only daytime variability between 8 am and 8 pm considered) and photographs summarizing the main
396 sink-source patterns in the landscape. Note that the southwestern corner of the study design has mountain birch
397 forest for which we did not have any data; we did not have measurements from the northeastern corner either.
398
399
400
401



402
403 **Figure 8:** Growing season mean and percentile (0.025 and 0.975) GHG fluxes in CO₂ equivalents based on in-
404 situ data and upscaled flux predictions, averaged across the entire study period (only daytime variability
405 between 8 am and 8 pm considered) and across vegetation types. Note that the scale for the x axis is different for
406 each gas species, and that the uncertainties in in-situ versus predicted mean fluxes cannot be directly compared
407 with each other. The uncertainty in in-situ wetland CH₄ continues up to 6.7 but was cropped for visualization
408 purposes. The same graph using the sustained GWP approach can be found in the Supplement Fig. 6 and
409 demonstrates the potentially larger role of CH₄ fluxes over a 100-year horizon in this landscape.

410 4 Discussion

411 4.1 CO₂ fluxes driven by both biotic and abiotic variables

412 Our results show the importance of several environmental variables for CO₂ fluxes, demonstrating the strong
413 dependence of GPP and ER on a wide range of soil microclimatological, hydrological, soil biogeochemical, and
414 ecological processes (Sørensen et al., 2019; Dagg and Lafleur, 2011; Nobrega and Grogan, 2008; Cahoon et al.,
415 2016). Overall, the relationships with environmental conditions and GPP and ER were rather similar.
416 Aboveground plant biomass and vegetation type were important drivers for both which suggests a dominance of
417 autotrophic (plant) respiration over heterotrophic (microbial) respiration. Biomass was a more important
418 predictor than vegetation type for all the CO₂ fluxes, indicating that the quantity of plant material producing and
419 emitting carbon was potentially more important than the different types of plants associated with CO₂ cycling in
420 this study setting (Happonen et al., 2022). The high importance of plant-related variables (e.g., leaf area index)
421 as drivers of spatial variability in CO₂ fluxes has been previously found in other tundra landscapes (Marushchak
422 et al. 2013 and references therein).



423

424 Our models also show that annual soil temperatures have a different and stronger relationship with CO₂ fluxes
425 than instantaneous growing season soil temperatures, and these two soil temperature variables are indeed
426 negatively correlated in this study design. This is because annual soil temperatures are driven by winter soil
427 temperatures which increase with thicker snow cover that is found particularly in the valley and in
428 microtopographic depressions, which are colder in the summer. Moreover, annual soil temperatures integrate
429 many other environmental conditions from the entire year: they reflect growing season length and temperature
430 conditions, regulate C and N availability, and control vegetation and microbial community composition and
431 functioning over long time scales. These conditions have been shown to be important drivers of CO₂ fluxes
432 across a range of Arctic sites (Zona et al., 2022; Lund et al., 2010). Similar to these previous studies, we
433 observed that plots with warmer annual soil conditions have larger growing season GPP and ER fluxes and
434 stronger net uptake. Our results also show other logical relationships between environmental conditions and CO₂
435 fluxes. For example, GPP and ER increased with soil moisture (Nobrega and Grogan, 2008). However, at
436 around 50-60 % VWC this relationship plateaued and turned negative. This was likely due to the lack of oxygen
437 causing plants to suffer and microbes to produce CH₄ instead of CO₂ in methanogenesis (Bridgman et al., 2013).
438 Further, soil organic carbon stock was an important predictor for ER, but not so much for GPP. This was likely
439 related to the higher soil carbon contents boosting decomposition (Schlesinger and Andrews, 2000).

440 **4.2 Small but consistent net CH₄ uptake mostly driven by soil moisture**

441 Net CH₄ flux was strongly controlled by soil moisture due to its effect on regulating the anoxic and oxic soil
442 conditions, and therefore CH₄ production (methanogenesis) and CH₄ consumption (CH₄ oxidation, or
443 methanotrophy) (Kelsey et al., 2016; Christensen et al., 1996; Treat et al., 2018b). Our results demonstrate that
444 the rate of CH₄ emissions increases sharply in water-logged soil conditions, i.e. at soil moisture levels of >60
445 VWC%. In drier conditions (VWC < 60%), soils contain more oxygen, which prevents CH₄ production and
446 increases net CH₄ uptake. This result supports findings from recent studies that show that drier upland tundra
447 areas can be habitats for methane oxidizing bacteria which can use CH₄ from the atmosphere as their main
448 energy source, transforming these environments to net CH₄ sinks (Christiansen et al., 2015; Juncher Jørgensen
449 et al., 2015; Lau et al., 2015; Emmerton et al., 2014; Wagner et al., 2019; St Pierre et al., 2019). Given the large
450 area of the Arctic, even minor fluxes such as those observed here for CH₄ uptake can be of global importance.
451 This CH₄ uptake can strengthen the GHG sink of the Arctic and prevent CH₄ from entering the atmosphere.

452

453 Our results show that net CH₄ uptake increases not only in drier conditions but also in soils with low C/N, soil
454 dissolved organic carbon, and carbon stocks. This is likely due to microbes needing and getting C and energy
455 from the atmosphere due to limited soil C supply (Lau et al., 2015; Juutinen et al., 2022), and the capability of
456 methanotrophs to effectively compete against classical heterotrophs dependent on larger organic
457 macromolecules in these environments. The models did not clearly identify a particular vegetation type
458 controlling net CH₄ uptake, however some individual models demonstrated deciduous shrubs and meadows to
459 be more closely related to net CH₄ uptake (Larmola et al., 2010). Overall, our results indicate that net CH₄
460 uptake potential is present in any kind of upland tundra vegetation type (Fig. S7) as long as the abiotic
461 conditions for microbes responsible for atmospheric CH₄ consumption are favourable.



462 CH₄ fluxes had a rather uniform distribution across the mineral upland regions (i.e., small but consistent net
463 uptake). High CH₄ emissions were located in wetland regions dominated by high soil organic carbon stocks and
464 moisture levels. Our observations demonstrated similar, or even higher net CH₄ uptake than previous studies.
465 For example, dry tundra was CH₄ neutral in a recent Arctic-Boreal CH₄ flux synthesis (mean=3.83, median= -
466 0.01 mg CH₄ m⁻² d⁻¹; primarily based on growing season daytime fluxes; Kuhn et al., 2021) whereas our study
467 showed higher uptake rates for the non-wetland plots (mean=-2.05, median=-1.81 mg CH₄ m⁻² d⁻¹). However,
468 studies focusing on individual sites have recorded similar CH₄ flux magnitudes as observed here (Emmertson et
469 al., 2014; Lau et al., 2015), but to the best of our knowledge, such extensive spatial patterns in CH₄ flux uptake
470 using fine spatial resolution models as presented here have not been published so far.

471 **4.3 N₂O fluxes remain neglectable and unpredictable**

472 We observed moderate, and to a large extent unpredictable variability in N₂O fluxes in this landscape. The
473 differences in average fluxes between the vegetation types were small. Based on our observations, most
474 vegetation types were on average N₂O sinks or neutral but deciduous and evergreen shrubs and meadows had
475 some variability from moderate N₂O sinks (up to -300 μg N m⁻² d⁻¹) to moderate N₂O sources (up to 400 μg N
476 m⁻² d⁻¹). Overall, our average N₂O fluxes were close to zero and thus low in the light of the recent review (Voigt
477 et al., 2020), which demonstrated that vegetated soils in permafrost regions are often small but evident sources
478 of N₂O during the growing season (~30 μg N m⁻² d⁻¹), and that barren or sparsely vegetated soils serve as
479 substantial sources of N₂O (~455 μg N m⁻² d⁻¹). The relatively small N₂O fluxes observed here can be explained
480 by the nitrogen-limited nature of the studied soils and the strong competition between plants and microbes for
481 nutrients: with low nitrogen stocks, nitrogen release by mineralization remains low (Voigt et al., 2020). Another
482 possible reason for the difference between our results and the synthesized N₂O flux estimates in Voigt et al.
483 2020 is that most of the data in the synthesis came from ecosystems that are not as much nitrogen-limited as our
484 site (e.g., peatlands, grasslands).

485
486 We were unable to explain the patterns in N₂O fluxes with the predictors used here. This was likely related to
487 the relatively low variability in N₂O fluxes in most of the plots in general, and the complexity of the soil
488 microbial N cycle, where N₂O is produced (nitrification, denitrification, DNRA) and consumed (denitrification)
489 by multiple co-occurring processes, differently regulated by environmental variables (Butterbach-Bahl et al.,
490 2013). Nevertheless, the most important driver of N₂O flux was soil C/N, and the models suggested that lower
491 C/N ratios were linked to higher net N₂O emissions. This is potentially due to the excess soil N allowing for
492 more rapid N mineralization, nitrification and denitrification which accelerate N₂O emissions (Klemetsson et
493 al., 2005; Liimatainen et al., 2018). Further, N₂O emissions were highest in the wetlands, similar to Ma et al.,
494 2007 who explained this by high ammonia or nitrate levels boosting N₂O production. The uppermost soil layers
495 were also likely not fully saturated by water at the time of the wetland measurements, which can induce higher
496 N₂O emissions in oxic conditions (Voigt et al., 2020; Takakai et al., 2008). In contrast to C fluxes, vegetation
497 type did not play an important role for N₂O fluxes. This might be related to our study having no measurements
498 in the previously observed, clear N₂O flux hot spots located in barren permafrost peatlands, such as peat
499 plateaus or palsas, with thick organic layers and high inorganic N content (Repo et al., 2009; Voigt et al.,
500 2017a).



501 **4.4 The sub-Arctic tundra landscape is a strong growing season GHG sink**

502 Our results demonstrate a high level of spatial heterogeneity in the growing season GHG fluxes across the
503 landscape, with all three gases acting as both net sinks and sources in some parts of it. Areas acting as GHG
504 sinks covered most of the landscape (CO₂: 92 %, CH₄: 95 %, N₂O: 64 %; 61 % of the area was a sink for all the
505 three GHGs). We observed clear differences in flux magnitudes driven by key environmental conditions. Moist,
506 and carbon and nitrogen-rich meadows and deciduous shrub heaths were strong GHG sinks. Wet sedge-
507 dominated fens were GHG sinks with CH₄ emissions being compensated by net CO₂ uptake. Barren lands and
508 evergreen shrubs were more resource-limited and closer to GHG neutral. These results are interesting in the
509 light of the shrubification patterns observed across the entire Arctic (Myers-Smith et al., 2011; Parker et al.,
510 2015; Vowles and Björk, 2018), and indicate that evergreen or deciduous shrub expansion may increase or
511 decrease the growing season GHG sink. If shrubs expand to meadows, the GHG sink may decrease, whereas if
512 they invade barren areas, the GHG sink may increase. However, our results did not quantify this change over
513 time, or cover the entire year to confirm the net annual effect.

514
515 Our results indicate that this heterogeneous Arctic landscape was a cumulative net GHG sink during the
516 measurement period during daytime (8 am to 8 pm) in July 2018. The July budget for CO₂ was -4.6 g C m⁻²
517 month⁻¹, for CH₄ -3.7 mg C m⁻² month⁻¹ and for N₂O -12.9 µg N m⁻² month⁻¹. The CO₂ sink is relatively small,
518 likely due to the high cover of patchy and sparsely vegetated areas that were often CO₂ sources. This small sink
519 value is likely an overestimation as we did not have measurements from the night time and did thus not upscale
520 fluxes in night-time conditions when ecosystems are net CO₂ sources due to the lack of light required for
521 photosynthesis. It also overestimates the importance of CO₂ as a radiative forcing agent, since ecosystem CO₂
522 production during autumn and winter contributes substantially to the annual C balance (Celis et al., 2017;
523 Commane et al., 2017), thereby reducing the CO₂ sink strength on an annual basis. Further, CH₄ uptake might
524 continue even in rather cold conditions as long as soils remain dry and unfrozen (Emmertson et al., 2014).
525 Nevertheless, our results demonstrate that net CO₂ uptake plays the most important role for the net growing
526 season GHG budget, but a small proportion of the GHG sink strength during growing season originates from net
527 CH₄ uptake. The role of N₂O fluxes for the net GHG budget across the entire landscape is negligible for the
528 growing season.

529 **4.5 Methodological considerations in GHG flux modeling**

530 Our study creates new understanding about high-resolution upscaling of GHG fluxes by incorporating more
531 chamber measurements, predictors, models, and environmental gradients compared to earlier efforts (see e.g.,
532 Fox et al., 2008; Dinsmore et al., 2017; Räsänen et al., 2021; Juutinen et al., 2022; Vainio et al., 2021). For
533 example, we included chamber measurements from 101 plots whereas earlier local-scale upscaling studies have
534 usually had circa 30 plots. Further, we included eight different environmental predictors while other studies
535 have often used only one or two, focusing on predictors describing vegetation type or soil moisture. Finally, we
536 studied a tundra landscape that consists of almost all the main vegetation types of the entire Arctic, whereas
537 earlier studies have investigated a narrower range of vegetation conditions, with a focus on wet ecosystems.

538



539 Our study showed that using means of in-situ GHG fluxes in each vegetation class to derive a landscape-level
540 GHG budget might produce significantly different results compared to the upscaled budget. This was apparent
541 particularly for CH₄ fluxes, where the in-situ based average wetland CH₄ emission was more than seven times
542 larger CH₄ compared to the upscaled one. This mismatch is likely explained by the heterogeneity of
543 environmental conditions and CH₄ fluxes within the wetland class that the chamber measurements alone could
544 not cover (Fig. S8). A multivariate machine learning modeling approach with variables describing not only
545 vegetation type but also soil moisture and other conditions were likely able to characterize the resulting CH₄
546 flux variability in a more representative way. For example, our soil moisture maps showed high variation in soil
547 moisture between ca. 50 and 70 VWC % within the wetland areas, and high CH₄ emissions were observed only
548 in areas with 60 VWC %. Overall, this result suggests that simple land cover-based upscaling efforts might lead
549 to biased budget estimates, especially when spatial variability within land cover types is high, emphasizing the
550 need for multivariate models in flux upscaling.

551
552 The performance of our models varied from good (GPP, CH₄ flux), moderate (ER and NEE) to low (N₂O). CH₄
553 fluxes - both sources and sinks - were most accurately modeled, providing important support for future studies
554 predicting not only the large CH₄ emissions but also the previously unquantified CH₄ uptake in Arctic
555 landscapes. The lower predictive performance of the models for other GHG fluxes might be explained by the
556 dynamic nature of fluxes not being represented in our spatial study design, and our models lacking important
557 predictors. The performance of the models could potentially be improved by describing plant functional
558 composition using plant traits (Happonen et al., 2022), and including more detailed information about soil
559 nutrients (e.g., soil nitrate or ammonium concentrations as soil C/N captures only very roughly how much N is
560 available) or microbial communities (e.g., communities or genes associated with nitrification or methanogenesis
561 or methanotrophy; Pessi et al., 2022).

562
563 We chose to use in-situ environmental data as predictors of GHG fluxes in our upscaling framework instead of
564 linking remotely sensed variables with GHG fluxes directly. This was done to increase understanding about the
565 mechanistic and ecological relationships but required us to first produce spatially continuous maps of
566 environmental conditions, which might have added an additional layer of uncertainty into our framework.
567 However, the most important environmental variables (i.e., soil moisture, temperature, biomass) had a high
568 predictive performance. Nevertheless, future studies could explore the performance and information derived by
569 upscaling GHG fluxes using high-resolution satellite or drone-derived remotely sensed indices directly (Siewert
570 and Olofsson, 2020; Vainio et al., 2021; Berner et al., 2018).

571
572 Overall, the performance of our machine learning models predicting spatial variability in GHG fluxes was
573 weaker than in other studies focusing on temporal variability (e.g., López-Blanco et al., 2017; Celis et al., 2017),
574 even though we had a comprehensive set of environmental measurements. Our results thus highlight the need
575 for more focus on the spatial patterns in GHG fluxes. While the temporal variability is widely acknowledged as
576 a source of uncertainty in GHG budget estimates (Baldocchi et al., 2018), the spatial variability may be just as
577 important but remains insufficiently studied (Treat et al., 2018c). Study designs focusing on spatial variation in
578 GHG fluxes using a combination of intensive measurement campaigns, remotely sensed datasets, and modeling



579 approaches are informative although they do not produce direct information on the trends and drivers of GHG
580 flux change following climate change. They provide new knowledge about the heterogeneity in GHG fluxes and
581 their environmental drivers which is highly important for understanding flux magnitudes from local to global
582 scales. Further, they can be used as a space-for-time substitution to understand ecosystem functions in locations
583 that are assumed to be at different stages of development. Moreover, this knowledge is valuable for designing
584 representative field studies in the future.

585

586 **5 Conclusions**

587 This study showed that predicting fluxes in heterogeneous tundra landscapes at high spatial resolutions is
588 possible for CH₄, GPP, and to some extent also NEE and ER fluxes but remains a challenge for N₂O fluxes. This
589 is a promising result for future high spatial resolution modeling studies that aim to understand the fine-scale
590 biogeochemistry of the rapidly changing Arctic environments. Our study further demonstrates high spatial
591 variability of GHG fluxes which is driven by a multitude of vegetation, soil microclimatological, hydrological,
592 and biogeochemical conditions. The upscaling shows the importance of net CO₂ uptake for the peak growing
593 season net GHG budget, and suggests that annual soil temperature and vegetation parameters are the most
594 important drivers. Most importantly, it reveals small but widespread CH₄ uptake across the entire upland tundra
595 in our domain that switches the studied landscape, consisting of wetlands with high CH₄ emissions, to a small
596 net CH₄ sink. This provides more evidence to the relatively unquantified but important CH₄ sink in the Arctic
597 GHG budget.

598 **Code/Data availability**

599 The field data, analysis codes and most of the results are available in a repository (Virkkala et al. 2023).
600 Upscaling results for each individual timestep were not included in the repository due to their large size, but
601 they can be acquired from the author upon request.

602 **Author contribution**

603 AMV and ML conceptualized the research with input from PN, JK, MEM, and CV. AMV, PN, JK, MEM, JK,
604 CV, GH, VT, JH and ML contributed to data collection. AMV analyzed the data and wrote the manuscript draft.
605 All the coauthors reviewed and edited the manuscript.

606 **Competing interests**

607 The authors declare no competing interests.



608 Acknowledgements

609 The authors would like to acknowledge the support by the research assistants during the data collection as well
610 as Kilpisjärvi Biological Station. AMV was supported by The Finnish Cultural Foundation, Alfred Kordelin
611 Foundation, Väisälä fund, and Jenny and Antti Wihuri Foundation, and the Gordon and Betty Moore foundation
612 (grant #8414). AMV and ML acknowledge the Academy of Finland funding (grant #286950). AMV and GH
613 acknowledge the Svenska Sällskapet för Antropologi och Geografi for funding. C.V. was supported by the
614 Academy of Finland project MUFFIN (no. 332196). ML acknowledges Academy of Finland funding (grant
615 #342890). C.B acknowledges funding from Academy of Finland general research grant (project N-PERM,
616 decision Nr. 341348). CB, CV, and MEM acknowledge Academy of Finland/Russian Foundation for Basic
617 Research project NOCA (decision no. 314630). PN was funded by the Academy of Finland (project number
618 347558). JK was funded by the Academy of Finland (project number 349606). JH was funded by the Academy
619 of Finland (grant #308128). We acknowledge funding for fieldwork and equipment by the Nordenskiöld
620 samfundet, Tiina and Antti Herlin foundation, and Maa- ja vesiteknikan tuki ry.

621 References

- 622 Agency, E. S.: Land Cover CCI Product User Guide Version 2 Tech. Rep, 2017.
- 623 Baldocchi, D., Chu, H., and Reichstein, M.: Inter-annual variability of net and gross ecosystem carbon fluxes: A
624 review, *Agric. For. Meteorol.*, 249, 520–533, <https://doi.org/10.1016/j.agrformet.2017.05.015>, 2018.
- 625 Belshe, E. F., Schuur, E. A. G., and Bolker, B. M.: Tundra ecosystems observed to be CO₂ sources due to
626 differential amplification of the carbon cycle, *Ecol. Lett.*, 16, 1307–1315, <https://doi.org/10.1111/ele.12164>,
627 2013.
- 628 Berner, L. T., Jantz, P., Tape, K. D., and Goetz, S. J.: Tundra plant above-ground biomass and shrub dominance
629 mapped across the North Slope of Alaska, *Environ. Res. Lett.*, 13, 035002, <https://doi.org/10.1088/1748-9326/aaaa9a>, 2018.
- 631 Bradley-Cook, J. I. and Virginia, R. A.: Landscape variation in soil carbon stocks and respiration in an Arctic
632 tundra ecosystem, west Greenland, *Arct. Antarct. Alp. Res.*, 50, S100024,
633 <https://doi.org/10.1080/15230430.2017.1420283>, 2018.
- 634 Breiman, L.: Random Forests, *Mach. Learn.*, 45, 5–32, <https://doi.org/10.1023/A:1010933404324>, 2001.
- 635 Bridgman, S. D., Cadillo-Quiroz, H., Keller, J. K., and Zhuang, Q.: Methane emissions from wetlands:
636 biogeochemical, microbial, and modeling perspectives from local to global scales, *Glob. Chang. Biol.*, 19,
637 1325–1346, <https://doi.org/10.1111/gcb.12131>, 2013.
- 638 Bruhwiler, L., Parmentier, F.-J. W., Crill, P., Leonard, M., and Palmer, P. I.: The Arctic Carbon Cycle and Its
639 Response to Changing Climate, *Current Climate Change Reports*, 7, 14–34, <https://doi.org/10.1007/s40641-020-00169-5>, 2021.
- 641 Brummell, M. E., Farrell, R. E., and Siciliano, S. D.: Greenhouse gas soil production and surface fluxes at a
642 high arctic polar oasis, *Soil Biol. Biochem.*, 52, 1–12, <https://doi.org/10.1016/j.soilbio.2012.03.019>, 2012.
- 643 Butterbach-Bahl, K., Baggs, E. M., Dannenmann, M., Kiese, R., and Zechmeister-Boltenstern, S.: Nitrous oxide
644 emissions from soils: how well do we understand the processes and their controls?, *Philos. Trans. R. Soc. Lond.*
645 *B Biol. Sci.*, 368, 20130122, <https://doi.org/10.1098/rstb.2013.0122>, 2013.
- 646 Cahoon, S. M. P., Sullivan, P. F., Shaver, G. R., Welker, J. M., Post, E., and Holyoak, M.: Interactions among
647 shrub cover and the soil microclimate may determine future Arctic carbon budgets, *Ecol. Lett.*, 15, 1415–1422,
648 <https://doi.org/10.1111/j.1461-0248.2012.01865.x>, 2012a.



- 649 Cahoon, S. M. P., Sullivan, P. F., Post, E., and Welker, J. M.: Large herbivores limit CO₂ uptake and suppress
650 carbon cycle responses to warming in West Greenland, *Glob. Chang. Biol.*, 18, 469–479,
651 <https://doi.org/10.1111/j.1365-2486.2011.02528.x>, 2012b.
- 652 Cahoon, S. M. P., Sullivan, P. F., and Post, E.: Greater Abundance of *Betula nana* and Early Onset of the
653 Growing Season Increase Ecosystem CO₂ Uptake in West Greenland, *Ecosystems*, 19, 1149–1163,
654 <https://doi.org/10.1007/s10021-016-9997-7>, 2016.
- 655 Celis, G., Mauritz, M., Bracho, R., Salmon, V. G., Webb, E. E., Hutchings, J., Natali, S. M., Schädel, C.,
656 Crummer, K. G., and Schuur, E. A. G.: Tundra is a consistent source of CO₂ at a site with progressive
657 permafrost thaw during 6 years of chamber and eddy covariance measurements,
658 <https://doi.org/10.1002/2016jg003671>, 2017.
- 659 Christensen, T. R., Prentice, I. C., Kaplan, J., Haxeltine, A., and Sitch, S.: Methane flux from northern wetlands
660 and tundra. An ecosystem source modelling approach, *Tellus B Chem. Phys. Meteorol.*, 48, 652–661,
661 <https://doi.org/10.1034/j.1600-0889.1996.t01-4-00004.x>, 1996.
- 662 Christiansen, J. R., Romero, A. J. B., Jørgensen, N. O. G., Glaring, M. A., Jørgensen, C. J., Berg, L. K., and
663 Elberling, B.: Methane fluxes and the functional groups of methanotrophs and methanogens in a young Arctic
664 landscape on Disko Island, West Greenland, *Biogeochemistry*, 122, 15–33, [https://doi.org/10.1007/s10533-014-](https://doi.org/10.1007/s10533-014-0026-7)
665 0026-7, 2015.
- 666 Commane, R., Lindaas, J., Benmergui, J., Luus, K. A., Chang, R. Y.-W., Daube, B. C., Euskirchen, E. S.,
667 Henderson, J. M., Karion, A., Miller, J. B., Miller, S. M., Parazoo, N. C., Randerson, J. T., Sweeney, C., Tans,
668 P., Thoning, K., Veraverbeke, S., Miller, C. E., and Wofsy, S. C.: Carbon dioxide sources from Alaska driven
669 by increasing early winter respiration from Arctic tundra, *Proc. Natl. Acad. Sci. U. S. A.*, 114, 5361–5366,
670 <https://doi.org/10.1073/pnas.1618567114>, 2017.
- 671 Dagg, J. and Lafleur, P.: Vegetation Community, Foliar Nitrogen, and Temperature Effects on Tundra CO₂
672 Exchange across a Soil Moisture Gradient, *Arct. Antarct. Alp. Res.*, 43, 189–197, [https://doi.org/10.1657/1938-](https://doi.org/10.1657/1938-4246-43.2.189)
673 4246-43.2.189, 2011.
- 674 Davidson, S. J., Santos, M. J., Sloan, V. L., Reuss-Schmidt, K., Phoenix, G. K., Oechel, W. C., and Zona, D.:
675 Upscaling CH₄ Fluxes Using High-Resolution Imagery in Arctic Tundra Ecosystems, *Remote Sensing*, 9, 1227,
676 <https://doi.org/10.3390/rs9121227>, 2017.
- 677 Dinerstein, E., Olson, D., Joshi, A., Vynne, C., Burgess, N. D., Wikramanayake, E., Hahn, N., Palminteri, S.,
678 Hedao, P., Noss, R., Hansen, M., Locke, H., Ellis, E. C., Jones, B., Barber, C. V., Hayes, R., Kormos, C.,
679 Martin, V., Crist, E., Sechrest, W., Price, L., Baillie, J. E. M., Weeden, D., Suckling, K., Davis, C., Sizer, N.,
680 Moore, R., Thau, D., Birch, T., Potapov, P., Turubanova, S., Tyukavina, A., de Souza, N., Pintea, L., Brito, J.
681 C., Llewellyn, O. A., Miller, A. G., Patzelt, A., Ghazanfar, S. A., Timberlake, J., Klöser, H., Shennan-Farpon,
682 Y., Kindt, R., Lillesø, J.-P. B., van Breugel, P., Graudal, L., Vogt, M., Al-Shammari, K. F., and Saleem, M.: An
683 Ecoregion-Based Approach to Protecting Half the Terrestrial Realm, *Bioscience*, 67, 534–545,
684 <https://doi.org/10.1093/biosci/bix014>, 2017.
- 685 Dinsmore, K. J., Drewer, J., Levy, P. E., George, C., Lohila, A., Aurela, M., and Skiba, U. M.: Growing season
686 CH₄ and N₂O fluxes from a subarctic landscape in northern Finland; from chamber to landscape scale,
687 <https://doi.org/10.5194/bg-14-799-2017>, 2017.
- 688 Emmerton, C. A., St. Louis, V. L., Lehnher, I., Humphreys, E. R., Rydz, E., and Kosolofski, H. R.: The net
689 exchange of methane with high Arctic landscapes during the summer growing season,
690 <https://doi.org/10.5194/bg-11-3095-2014>, 2014.
- 691 Euskirchen, E. S., Bret-Harte, M. S., Scott, G. J., Edgar, C., and Shaver, G. R.: Seasonal patterns of carbon
692 dioxide and water fluxes in three representative tundra ecosystems in northern Alaska, *Ecosphere*, 3, art4,
693 <https://doi.org/10.1890/es11-00202.1>, 2012.
- 694 Euskirchen, E. S., Edgar, C. W., Turetsky, M. R., Waldrop, M. P., and Harden, J. W.: Differential response of
695 carbon fluxes to climate in three peatland ecosystems that vary in the presence and stability of permafrost, *J.*
696 *Geophys. Res. Biogeosci.*, 119, 1576–1595, <https://doi.org/10.1002/2014jg002683>, 2014.
- 697 Fox, A. M., Huntley, B., Lloyd, C. R., Williams, M., and Baxter, R.: Net ecosystem exchange over



- 698 heterogeneous Arctic tundra: Scaling between chamber and eddy covariance measurements, *Global*
699 *Biogeochem. Cycles*, 22, 2008.
- 700 Frohking, S., Roulet, N., and Fuglestedt, J.: How northern peatlands influence the Earth's radiative budget:
701 Sustained methane emission versus sustained carbon sequestration, *J. Geophys. Res.*, 111,
702 <https://doi.org/10.1029/2005jg000091>, 2006.
- 703 Greenwell, B., Brandon, Greenwell, M., Bradley, and Boehmke, C.: Variable Importance Plots—An
704 Introduction to the vip Package, <https://doi.org/10.32614/rj-2020-013>, 2020.
- 705 Greenwell, B. M.: pdp: An R Package for Constructing Partial Dependence Plots, *R J.*, 9, 421, 2017.
- 706 Happonen, K., Virkkala, A.-M., Kemppinen, J., Niittynen, P., and Luoto, M.: Relationships between above-
707 ground plant traits and carbon cycling in tundra plant communities, *J. Ecol.*, 110, 700–716, 2022.
- 708 Heiskanen, L., Tuovinen, J.-P., Räsänen, A., Virtanen, T., Juutinen, S., Lohila, A., Penttilä, T., Linkosalmi, M.,
709 Mikola, J., Laurila, T., and Aurela, M.: Carbon dioxide and methane exchange of a patterned subarctic fen
710 during two contrasting growing seasons, *Biogeosciences*, 18, 873–896, <https://doi.org/10.5194/bg-18-873-2021>,
711 2021.
- 712 Hensgens, G., Laudon, H., Johnson, M. S., and Berggren, M.: The undetected loss of aged carbon from boreal
713 mineral soils, *Sci. Rep.*, 11, 6202, <https://doi.org/10.1038/s41598-021-85506-w>, 2021.
- 714 Hugelius, G., Strauss, J., Zubrzycki, S., Harden, J. W., Schuur, E. A. G., Ping, C.-L., Schirmer, L., Grosse,
715 G., Michaelson, G. J., Koven, C. D., and Others: Estimated stocks of circumpolar permafrost carbon with
716 quantified uncertainty ranges and identified data gaps, *Biogeosciences*, 11, 2014.
- 717 Hugelius, G., Loisel, J., Chadburn, S., Jackson, R. B., Jones, M., MacDonald, G., Marushchak, M., Olefeldt, D.,
718 Packalen, M., Siewert, M. B., Treat, C., Turetsky, M., Voigt, C., and Yu, Z.: Large stocks of peatland carbon
719 and nitrogen are vulnerable to permafrost thaw, *Proc. Natl. Acad. Sci. U. S. A.*, 117, 20438–20446,
720 <https://doi.org/10.1073/pnas.1916387117>, 2020.
- 721 Juncher Jørgensen, C., Lund Johansen, K. M., Westergaard-Nielsen, A., and Elberling, B.: Net regional methane
722 sink in High Arctic soils of northeast Greenland, *Nat. Geosci.*, 8, 20–23, <https://doi.org/10.1038/ngeo2305>,
723 2015.
- 724 Juutinen, S., Aurela, M., Tuovinen, J.-P., Ivakhov, V., Linkosalmi, M., Räsänen, A., Virtanen, T., Mikola, J.,
725 Nyman, J., Vähä, E., Loskutova, M., Makshtas, A., and Laurila, T.: Variation in CO₂ and CH₄ fluxes among
726 land cover types in heterogeneous Arctic tundra in northeastern Siberia, *Biogeosciences*, 19, 3151–3167,
727 <https://doi.org/10.5194/bg-19-3151-2022>, 2022.
- 728 Kåresdotter, E., Destouni, G., Ghajarnia, N., Hugelius, G., and Kalantari, Z.: Mapping the vulnerability of arctic
729 wetlands to global warming, *Earth's Future*, 9, <https://doi.org/10.1029/2020ef001858>, 2021.
- 730 Kelsey, K. C., Leffler, A. J., Beard, K. H., Schmutz, J. A., Choi, R. T., and Welker, J. M.: Interactions among
731 vegetation, climate, and herbivory control greenhouse gas fluxes in a subarctic coastal wetland, *Journal of*
732 *Geophysical Research: Biogeosciences*, 121, 2960–2975, 2016.
- 733 Kemppinen, J., Niittynen, P., Virkkala, A.-M., Happonen, K., Riihimäki, H., Aalto, J., and Luoto, M.: Dwarf
734 Shrubs Impact Tundra Soils: Drier, Colder, and Less Organic Carbon, *Ecosystems*,
735 <https://doi.org/10.1007/s10021-020-00589-2>, 2021.
- 736 King, L. and Seppälä, M.: Permafrost thickness and distribution in Finnish Lapland—Results of geoelectrical
737 soundings, *Polarforschung*, 57, 127–147, 1987.
- 738 Klemmedtsson, L., Von Arnold, K., Weslien, P., and Gundersen, P.: Soil CN ratio as a scalar parameter to predict
739 nitrous oxide emissions, *Glob. Chang. Biol.*, 11, 1142–1147, <https://doi.org/10.1111/j.1365-2486.2005.00973.x>,
740 2005.
- 741 Kuhn, M. A., Varner, R. K., Bastviken, D., Crill, P., MacIntyre, S., Turetsky, M., Walter Anthony, K., McGuire,
742 A. D., and Olefeldt, D.: BAWLD-CH 4: a comprehensive dataset of methane fluxes from boreal and arctic
743 ecosystems, *Earth System Science Data*, 13, 5151–5189, 2021.



- 744 Larmola, T., Tuittila, E.-S., Tirola, M., Nykänen, H., Martikainen, P. J., Yrjälä, K., Tuomivirta, T., and Fritze,
745 H.: The role of Sphagnum mosses in the methane cycling of a boreal mire, *Ecology*, 91, 2356–2365,
746 <https://doi.org/10.1890/09-1343.1>, 2010.
- 747 Lau, M. C. Y., Stackhouse, B. T., Layton, A. C., Chauhan, A., Vishnivetskaya, T. A., Chourey, K., Ronholm, J.,
748 Mykityczuk, N. C. S., Bennett, P. C., Lamarche-Gagnon, G., Burton, N., Pollard, W. H., Omelon, C. R.,
749 Medvigy, D. M., Hettich, R. L., Pfiffner, S. M., Whyte, L. G., and Onstott, T. C.: An active atmospheric
750 methane sink in high Arctic mineral cryosols, *ISME J.*, 9, 1880–1891, <https://doi.org/10.1038/ismej.2015.13>,
751 2015.
- 752 Liimatainen, M., Voigt, C., Martikainen, P. J., Hytönen, J., Regina, K., Óskarsson, H., and Maljanen, M.:
753 Factors controlling nitrous oxide emissions from managed northern peat soils with low carbon to nitrogen ratio,
754 *Soil Biol. Biochem.*, 122, 186–195, <https://doi.org/10.1016/j.soilbio.2018.04.006>, 2018.
- 755 Livingston, G. P. and Hutchingson, G. L.: Enclosure-based measurement of trace gas exchange: applications
756 and sources of error.[Bokförf.], 1995.
- 757 López-Blanco, E., Lund, M., Williams, M., Tamstorf, M. P., Westergaard-Nielsen, A., Exbrayat, J.-F., Hansen,
758 B. U., and Christensen, T. R.: Exchange of CO₂ in Arctic tundra: impacts of meteorological variations and
759 biological disturbance, *Biogeosciences*, 14, 4467, 2017.
- 760 Lund, M., Lafleur, P. M., Roulet, N. T., Lindroth, A., Christensen, T. R., Aurela, M., Chojnicki, B. H.,
761 Flanagan, L. B., Humphreys, E. R., Laurila, T., Oechel, W. C., Olejnik, J., Rinne, J., Schubert, P., and Nilsson,
762 M. B.: Variability in exchange of CO₂ across 12 northern peatland and tundra sites, *Glob. Chang. Biol.*, 16,
763 2436–2448, <https://doi.org/10.1111/j.1365-2486.2009.02104.x>, 2010.
- 764 Magnani, M., Baneschi, I., Giamberini, M., Raco, B., and Provenzale, A.: Microscale drivers of summer CO₂
765 fluxes in the Svalbard High Arctic tundra, *Sci. Rep.*, 12, 763, <https://doi.org/10.1038/s41598-021-04728-0>,
766 2022.
- 767 Masyagina, O. V. and Menyailo, O. V.: The impact of permafrost on carbon dioxide and methane fluxes in
768 Siberia: A meta-analysis, *Environ. Res.*, 182, 109096, <https://doi.org/10.1016/j.envres.2019.109096>, 2020.
- 769 Mathijssen, P. J. H., Tuovinen, J.-P., Lohila, A., Väliänta, M., and Tuittila, E.-S.: Identifying main uncertainties
770 in estimating past and present radiative forcing of peatlands, *Glob. Chang. Biol.*, 28, 4069–4084,
771 <https://doi.org/10.1111/gcb.16189>, 2022.
- 772 Mauritz, M., Bracho, R., Celis, G., Hutchings, J., Natali, S. M., Pegoraro, E., Salmon, V. G., Schädel, C., Webb,
773 E. E., and Schuur, E. A. G.: Nonlinear CO₂ flux response to 7 years of experimentally induced permafrost thaw,
774 *Glob. Chang. Biol.*, 23, 3646–3666, <https://doi.org/10.1111/gcb.13661>, 2017.
- 775 Ma, W. K., Schautz, A., Fishback, L.-A. E., Bedard-Haughn, A., Farrell, R. E., and Siciliano, S. D.: Assessing
776 the potential of ammonia oxidizing bacteria to produce nitrous oxide in soils of a high arctic lowland ecosystem
777 on Devon Island, Canada, *Soil Biol. Biochem.*, 39, 2001–2013, <https://doi.org/10.1016/j.soilbio.2007.03.001>,
778 2007.
- 779 McGuire, A. D., Christensen, T. R., Hayes, D. J., Heroult, A., Euskirchen, E., Yi, Y., Kimball, J. S., Koven, C.,
780 Lafleur, P., Miller, P. A., Oechel, W., Peylin, P., and Williams, M.: An assessment of the carbon balance of
781 arctic tundra: comparisons among observations, process models, and atmospheric inversions, *Biogeosci.*
782 *Discuss.*, 9, 4543, <https://doi.org/10.5194/bg-9-3185-2012>, 2012.
- 783 Myers-Smith, I. H., Forbes, B. C., Wilmsking, M., Hallinger, M., Lantz, T., Blok, D., Tape, K. D., Macias-
784 Fauria, M., Sass-Klaassen, U., Lévesque, E., Boudreau, S., Ropars, P., Hermanutz, L., Trant, A., Collier, L. S.,
785 Weijers, S., Rozema, J., Rayback, S. A., Schmidt, N. M., Schaepman-Strub, G., Wipf, S., Rixen, C., Ménard, C.
786 B., Venn, S., Goetz, S., Andreu-Hayles, L., Elmendorf, S., Ravolainen, V., Welker, J., Grogan, P., Epstein, H.
787 E., and Hik, D. S.: Shrub expansion in tundra ecosystems: dynamics, impacts and research priorities,
788 <https://doi.org/10.1088/1748-9326/6/4/045509>, 2011.
- 789 Natali, S. M., Watts, J. D., Rogers, B. M., Potter, S., Ludwig, S. M., Selbmann, A.-K., Sullivan, P. F., Abbott, B.
790 W., Arndt, K. A., Birch, L., Björkman, M. P., Bloom, A. A., Celis, G., Christensen, T. R., Christiansen, C. T.,
791 Commane, R., Cooper, E. J., Crill, P., Czimeczik, C., Davydov, S., Du, J., Egan, J. E., Elberling, B., Euskirchen,
792 E. S., Friborg, T., Genet, H., Göckede, M., Goodrich, J. P., Grogan, P., Helbig, M., Jafarov, E. E., Jastrow, J. D.,



- 793 Kalhori, A. A. M., Kim, Y., Kimball, J. S., Kutzbach, L., Lara, M. J., Larsen, K. S., Lee, B.-Y., Liu, Z., Loranty,
794 M. M., Lund, M., Lupascu, M., Madani, N., Malhotra, A., Matamala, R., McFarland, J., McGuire, A. D.,
795 Michelsen, A., Minions, C., Oechel, W. C., Olefeldt, D., Parmentier, F.-J. W., Pirk, N., Poulter, B., Quinton, W.,
796 Rezanezhad, F., Risk, D., Sachs, T., Schaefer, K., Schmidt, N. M., Schuur, E. A. G., Semenchuk, P. R., Shaver,
797 G., Sonntag, O., Starr, G., Treat, C. C., Waldrop, M. P., Wang, Y., Welker, J., Wille, C., Xu, X., Zhang, Z.,
798 Zhuang, Q., and Zona, D.: Large loss of CO₂ in winter observed across the northern permafrost region, *Nat.*
799 *Clim. Chang.*, 9, 852–857, <https://doi.org/10.1038/s41558-019-0592-8>, 2019.
- 800 National Land Survey of Finland. 2019. Digital elevation model. National Land Survey of Finland.
801 [https://www.maanmittauslaitos.fi/en/maps-and-spatial-data/expert-users/product-descriptions/elevation-model-](https://www.maanmittauslaitos.fi/en/maps-and-spatial-data/expert-users/product-descriptions/elevation-model-2-m)
802 [2-m](https://www.maanmittauslaitos.fi/en/maps-and-spatial-data/expert-users/product-descriptions/elevation-model-2-m). Last accessed 19/04/2019
803
- 804 Nobrega, S. and Grogan, P.: Landscape and ecosystem-level controls on net carbon dioxide exchange along a
805 natural moisture gradient in Canadian low arctic tundra, *Ecosystems*, 11, 377–396,
806 <https://doi.org/10.1007/s10021-008-9128-1>, 2008.
- 807 Olefeldt, D., Hovemyr, M., Kuhn, M. A., Bastviken, D., Bohn, T. J., Connolly, J., Crill, P., Euskirchen, E. S.,
808 Finkelstein, S. A., Genet, H., Grosse, G., Harris, L. I., Heffernan, L., Helbig, M., Hugelius, G., Hutchins, R.,
809 Juutinen, S., Lara, M. J., Malhotra, A., Manies, K., McGuire, A. D., Natali, S. M., O'Donnell, J. A., Parmentier,
810 F.-J. W., Räsänen, A., Schädel, C., Sonntag, O., Strack, M., Tank, S. E., Treat, C., Varner, R. K., Virtanen, T.,
811 Warren, R. K., and Watts, J. D.: The boreal–Arctic Wetland and Lake Dataset (BAWLD), *Earth Syst. Sci. Data*,
812 13, 5127–5149, <https://doi.org/10.5194/essd-13-5127-2021>, 2021.
- 813 Pallandt, M., Kumar, J., Mauritz, M., Schuur, E., Virkkala, A.-M., Celis, G., Hoffman, F., and Göckede, M.:
814 Representativeness assessment of the pan-Arctic eddy-covariance site network, and optimized future
815 enhancements, *Biogeosciences*, <https://doi.org/10.5194/bg-2021-133>, 2021.
- 816 Parker, T. C., Subke, J.-A., and Wookey, P. A.: Rapid carbon turnover beneath shrub and tree vegetation is
817 associated with low soil carbon stocks at a subarctic treeline, *Glob. Chang. Biol.*, 21, 2070–2081,
818 <https://doi.org/10.1111/gcb.12793>, 2015.
- 819 Peltola, O., Vesala, T., Gao, Y., Rätty, O., Alekseychik, P., Aurela, M., Chojnicki, B., Desai, A. R., Dolman, A.
820 J., Euskirchen, E. S., Friborg, T., Göckede, M., Helbig, M., Humphreys, E., Jackson, R. B., Jocher, G., Joos, F.,
821 Klatt, J., Knox, S. H., Kowalska, N., Kutzbach, L., Lienert, S., Lohila, A., Mammarella, I., Nadeau, D. F.,
822 Nilsson, M. B., Oechel, W. C., Peichl, M., Pypker, T., Quinton, W., Rinne, J., Sachs, T., Samson, M., Schmid,
823 H. P., Sonntag, O., Wille, C., Zona, D., and Aalto, T.: Monthly gridded data product of northern wetland
824 methane emissions based on upscaling eddy covariance observations, *Earth System Science Data*, 11, 1263–
825 1289, <https://doi.org/10.5194/essd-11-1263-2019>, 2019.
- 826 Pessi, I. S., Viitamäki, S., Virkkala, A.-M., Eronen-Rasimus, E., Delmont, T. O., Marushchak, M. E., Luoto, M.,
827 and Hultman, J.: In-depth characterization of denitrifier communities across different soil ecosystems in the
828 tundra, *Environ Microbiome*, 17, 30, <https://doi.org/10.1186/s40793-022-00424-2>, 2022.
- 829 R Core Team (2020). R: A language and environment for statistical computing. R Foundation for Statistical
830 Computing, Vienna, Austria. <https://www.R-project.org/>.
- 831 Räsänen, A., Manninen, T., Korkiakoski, M., Lohila, A., and Virtanen, T.: Predicting catchment-scale methane
832 fluxes with multi-source remote sensing, *Landsc. Ecol.*, 36, 1177–1195, [https://doi.org/10.1007/s10980-021-](https://doi.org/10.1007/s10980-021-833)
833 [01194-x](https://doi.org/10.1007/s10980-021-833), 2021.
- 834 Reynolds, M. K., Walker, D. A., Balsler, A., Bay, C., Campbell, M., Cherosov, M. M., Daniëls, F. J. A., Eidesen,
835 P. B., Ermokhina, K. A., Frost, G. V., Jedrzejek, B., Jorgenson, M. T., Kennedy, B. E., Kholod, S. S.,
836 Lavrinenko, I. A., Lavrinenko, O. V., Magnússon, B., Matveyeva, N. V., Metúsalemsson, S., Nilsen, L., Olthof,
837 I., Pospelov, I. N., Pospelova, E. B., Pouliot, D., Razzhivin, V., Schaepman-Strub, G., Šibík, J., Telyatnikov, M.
838 Y., and Troeva, E.: A raster version of the Circumpolar Arctic Vegetation Map (CAVM), *Remote Sens.*
839 *Environ.*, 232, 111297, <https://doi.org/10.1016/j.rse.2019.111297>, 2019.
- 840 Repo, M. E., Susiluoto, S., Lind, S. E., Jokinen, S., Elsakov, V., Biasi, C., Virtanen, T., and Martikainen, P. J.:
841 Large N₂O emissions from cryoturbated peat soil in tundra, *Nat. Geosci.*, 2, 189–192,
842 <https://doi.org/10.1038/ngeo434>, 2009.
- 843 Rinne, J., Tuittila, E.-S., Peltola, O., Li, X., Raivonen, M., Alekseychik, P., Haapanala, S., Pihlatie, M., Aurela,



- 844 M., Mammarella, I., and Vesala, T.: Temporal Variation of Ecosystem Scale Methane Emission From a Boreal
845 Fen in Relation to Temperature, Water Table Position, and Carbon Dioxide Fluxes, *Global Biogeochem. Cycles*,
846 32, 1087–1106, <https://doi.org/10.1029/2017GB005747>, 2018.
- 847 Schlesinger, W. H. and Andrews, J. A.: Soil respiration and the global carbon cycle, *Biogeochemistry*, 48, 7–20,
848 <https://doi.org/10.1023/A:1006247623877>, 2000.
- 849 Shaver, G. R., L. E. Street, Rastetter, E. B., M. T. Van Wijk, and Williams, M.: Functional Convergence in
850 Regulation of Net CO₂ Flux in Heterogeneous Tundra Landscapes in Alaska and Sweden, *J. Ecol.*, 95, 802–817,
851 2007.
- 852 Siewert, M. B. and Olofsson, J.: Scale-dependency of Arctic ecosystem properties revealed by UAV, *Environ.*
853 *Res. Lett.*, 15, 094030, <https://doi.org/10.1088/1748-9326/aba20b>, 2020.
- 854 Sørensen, M. V., Graae, B. J., Classen, A., Enquist, B. J., and Strimbeck, R.: Drivers of C cycling in three
855 arctic-alpine plant communities, *Arct. Antarct. Alp. Res.*, 51, 128–147,
856 <https://doi.org/10.1080/15230430.2019.1592649>, 2019.
- 857 St Pierre, K. A., Danielsen, B. K., Hermesdorf, L., D’Imperio, L., Iversen, L. L., and Elberling, B.: Drivers of
858 net methane uptake across Greenlandic dry heath tundra landscapes, *Soil Biol. Biochem.*, 138, 107605,
859 <https://doi.org/10.1016/j.soilbio.2019.107605>, 2019.
- 860 Strauss, J., Schirrmester, L., Grosse, G., Fortier, D., Hugelius, G., Knoblauch, C., Romanovsky, V., Schädel,
861 C., Schneider von Deimling, T., Schuur, E. A. G., Shmelev, D., Ulrich, M., and Veremeeva, A.: Deep Yedoma
862 permafrost: A synthesis of depositional characteristics and carbon vulnerability, *Earth-Sci. Rev.*, 172, 75–86,
863 <https://doi.org/10.1016/j.earscirev.2017.07.007>, 2017.
- 864 Takakai, F., Desyatkin, A. R., Lopez, C. M. L., Fedorov, A. N., Desyatkin, R. V., and Hatano, R.: CH₄ and N₂O
865 emissions from a forest-alas ecosystem in the permafrost taiga forest region, eastern Siberia, Russia, *J. Geophys.*
866 *Res.*, 113, <https://doi.org/10.1029/2007jg000521>, 2008.
- 867 Tramontana, G., Jung, M., Schwalm, C. R., Ichii, K., Camps-Valls, G., Ráduly, B., Reichstein, M., Arain, M.
868 A., Cescatti, A., Kiely, G., and Others: Predicting carbon dioxide and energy fluxes across global FLUXNET
869 sites with regression algorithms, *Biogeosciences*, 13, 4291–4313, 2016.
- 870 Treat, C. C., Anthony Bloom, A., and Marushchak, M. E.: Nongrowing season methane emissions—a significant
871 component of annual emissions across northern ecosystems, <https://doi.org/10.1111/gcb.14137>, 2018a.
- 872 Treat, C. C., Bloom, A. A., and Marushchak, M. E.: Nongrowing season methane emissions—a significant
873 component of annual emissions across northern ecosystems, *Glob. Chang. Biol.*, 24, 3331–3343, 2018b.
- 874 Treat, C. C., Marushchak, M. E., Voigt, C., Zhang, Y., Tan, Z., Zhuang, Q., Virtanen, T. A., Räsänen, A., Biasi,
875 C., Hugelius, G., Kaverin, D., Miller, P. A., Stendel, M., Romanovsky, V., Rivkin, F., Martikainen, P. J., and
876 Shurpali, N. J.: Tundra landscape heterogeneity, not interannual variability, controls the decadal regional carbon
877 balance in the Western Russian Arctic, *Glob. Chang. Biol.*, 24, 5188–5204, <https://doi.org/10.1111/gcb.14421>,
878 2018c.
- 879 Turetsky, M. R., Kotowska, A., Bubier, J., Dise, N. B., Crill, P., Hornibrook, E. R. C., Minkinen, K., Moore, T.
880 R., Myers-Smith, I. H., Nykänen, H., Olefeldt, D., Rinne, J., Saarnio, S., Shurpali, N., Tuittila, E.-S.,
881 Waddington, J. M., White, J. R., Wickland, K. P., and Wilmking, M.: A synthesis of methane emissions from 71
882 northern, temperate, and subtropical wetlands, *Glob. Chang. Biol.*, 20, 2183–2197,
883 <https://doi.org/10.1111/gcb.12580>, 2014.
- 884 Tyystjärvi, V., Kemppinen, J., Luoto, M., Aalto, T., Markkanen, T., Launiainen, S., Kieloaho, A.-J., and Aalto,
885 J.: Modelling spatio-temporal soil moisture dynamics in mountain tundra, *Hydrol. Process.*, 36,
886 <https://doi.org/10.1002/hyp.14450>, 2022.
- 887 Vainio, E., Peltola, O., Kasurinen, V., Kieloaho, A.-J., Tuittila, E.-S., and Pihlatie, M.: Topography-based
888 statistical modelling reveals high spatial variability and seasonal emission patches in forest floor methane flux,
889 *Biogeosciences*, 18, 2003–2025, <https://doi.org/10.5194/bg-18-2003-2021>, 2021.
- 890 Virkkala, A.-M., Virtanen, T., Lehtonen, A., Rinne, J., and Luoto, M.: The current state of CO₂ flux chamber



- 891 studies in the Arctic tundra: A review, *Progress in Physical Geography: Earth and Environment*, 42, 162–184,
892 <https://doi.org/10.1177/0309133317745784>, 2018.
- 893 Virkkala, A.-M., Aalto, J., Rogers, B. M., Tagesson, T., Treat, C. C., Natali, S. M., Watts, J. D., Potter, S.,
894 Lehtonen, A., Mauritz, M., Schuur, E. A. G., Kochendorfer, J., Zona, D., Oechel, W., Kobayashi, H.,
895 Humphreys, E., Goeckede, M., Iwata, H., Lafleur, P. M., Euskirchen, E. S., Bokhorst, S., Marushchak, M.,
896 Martikainen, P. J., Elberling, B., Voigt, C., Biasi, C., Sonnentag, O., Parmentier, F.-J. W., Ueyama, M., Celis,
897 G., St Loius, V. L., Emmerton, C. A., Peichl, M., Chi, J., Järveoja, J., Nilsson, M. B., Oberbauer, S. F., Torn, M.
898 S., Park, S.-J., Dolman, H., Mammarella, I., Chae, N., Poyatos, R., López-Blanco, E., Røjle Christensen, T.,
899 Jung Kwon, M., Sachs, T., Holl, D., and Luoto, M.: Statistical upscaling of ecosystem CO₂ fluxes across the
900 terrestrial tundra and boreal domain: regional patterns and uncertainties, *Glob. Chang. Biol.*,
901 <https://doi.org/10.1111/gcb.15659>, 2021.
- 902 Virkkala, A.-M., Niittynen, P., Kemppinen, J., Marushchak, M.E, Voigt, C., Hensgens, G., Kerttula, J., Happonen,
903 K., Tyystjärvi, V., Biasi, C., Hultman, J., Rinne, J., & Luoto, M. Data and code for "High-resolution spatial
904 patterns and drivers of terrestrial ecosystem carbon dioxide, methane, and nitrous oxide fluxes in the tundra" [Data
905 set]. Zenodo. <https://doi.org/10.5281/zenodo.7760577>, 2023.
- 906
907 Voigt, C., Marushchak, M. E., Lamprecht, R. E., Jackowicz-Korczyński, M., Lindgren, A., Mastepanov, M.,
908 Granlund, L., Christensen, T. R., Tahvanainen, T., Martikainen, P. J., and Biasi, C.: Increased nitrous oxide
909 emissions from Arctic peatlands after permafrost thaw, *Proc. Natl. Acad. Sci. U. S. A.*, 114, 6238–6243,
910 <https://doi.org/10.1073/pnas.1702902114>, 2017a.
- 911 Voigt, C., Lamprecht, R. E., Marushchak, M. E., Lind, S. E., Novakovskiy, A., Aurela, M., Martikainen, P. J.,
912 and Biasi, C.: Warming of subarctic tundra increases emissions of all three important greenhouse gases--carbon
913 dioxide, methane, and nitrous oxide, *Glob. Chang. Biol.*, 23, 3121–3138, 2017b.
- 914 Voigt, C., Marushchak, M. E., Abbott, B. W., Biasi, C., Elberling, B., Siciliano, S. D., Sonnentag, O., Stewart,
915 K. J., Yang, Y., and Martikainen, P. J.: Nitrous oxide emissions from permafrost-affected soils, *Nature Reviews*
916 *Earth & Environment*, 1, 420–434, <https://doi.org/10.1038/s43017-020-0063-9>, 2020.
- 917 Vowles, T. and Björk, R. G.: Implications of evergreen shrub expansion in the Arctic, *J. Ecol.*, 107, 650–655,
918 <https://doi.org/10.1111/1365-2745.13081>, 2018.
- 919 Wagner, I., Hung, J. K. Y., Neil, A., and Scott, N. A.: Net greenhouse gas fluxes from three High Arctic plant
920 communities along a moisture gradient, *Arct. sci.*, 5, 185–201, <https://doi.org/10.1139/as-2018-0018>, 2019.
- 921 Wild, J., Kopecký, M., Macek, M., Šanda, M., Jankovec, J., and Haase, T.: Climate at ecologically relevant
922 scales: A new temperature and soil moisture logger for long-term microclimate measurement, *Agric. For.*
923 *Meteorol.*, 268, 40–47, <https://doi.org/10.1016/j.agrformet.2018.12.018>, 2019.
- 924 Williams, M., Street, L. E., van Wijk, M. T., and Shaver, G. R.: Identifying Differences in Carbon Exchange
925 among Arctic Ecosystem Types, *Ecosystems*, 9, 288–304, <https://doi.org/10.1007/s10021-005-0146-y>, 2006.
- 926 Zona, D., Lafleur, P. M., Hufkens, K., Bailey, B., Gioli, B., Burba, G., Goodrich, J. P., Liljedahl, A. K.,
927 Euskirchen, E. S., Watts, J. D., Farina, M., Kimball, J. S., Heimann, M., Goeckede, M., Pallandt, M.,
928 Christensen, T. R., Mastepanov, M., López-Blanco, E., Jackowicz-Korczynski, M., Dolman, A. J., Marchesini,
929 L. B., Commare, R., Wofsy, S. C., Miller, C. E., Lipson, D. A., Hashemi, J., Arndt, K. A., Kutzbach, L., Holl,
930 D., Boike, J., Wille, C., Sachs, T., Kalhori, A., Song, X., Xu, X., Humphreys, E. R., Koven, C. D., Sonnentag,
931 O., Meyer, G., Gosselin, G. H., Marsh, P., and Oechel, W. C.: Earlier snowmelt may lead to late season declines
932 in plant productivity and carbon sequestration in Arctic tundra ecosystems, *Sci. Rep.*, 12, 3986,
933 <https://doi.org/10.1038/s41598-022-07561-1>, 2022.
- 934
935
936
937
938
939
940
941